Manuscript Number:	PALAEO-D-21-00105
Article Type:	39_VSI:Palaeosols and Sediments
Keywords:	Paleosol stratigraphy; pedo-sedimentary evolution; radiocarbon dates; climate change; eustasy; Late Quaternary
Corresponding Author:	Luigi Bruno University of Modena and Reggio Emilia: Universita degli Studi di Modena e Reggio Emilia ITALY
First Author:	Luigi Bruno
Order of Authors:	Luigi Bruno
	Bruno Campo
	Irka Hajdas
	Wan Hong
	Alessandro Amorosi
Manuscript Region of Origin:	Europe
Abstract:	Paleosol stratigraphy in the Po Plain, reconstructed through sedimentological analysis and correlation of ca. 170 core data chronologically constrained by 376 radiocarbon dates, revealed strict relationships between pedogenetic and fluvial processes in alluvial and paralic environments. Vertically stacked, weakly developed paleosols within Upper Pleistocene and Holocene mud-prone strata testify to intermittent pedogenesis, periodically interrupted by overbank sedimentation. Individual paleosols are laterally traceable for tens of km and exhibit A-Bk-Bw, A-Bk or A-Bw profiles. Stratigraphically ordered 14C calibrated ages from A horizons testify to slow aggradation during 4-6 thousand years-long exposure periods. Burial ages, with an error of few centuries, are provided by plant debris at the top of A horizons. Millennial-scale climate oscillations and glacio-eustasy are the main drivers of the pedo-sedimentary evolution of the area during the last 50 kyr. Pleistocene (P) paleosols developed in well-drained floodplain environments, dissected by fluvial incision, during relatively warm periods. Overbank sedimentation and paleosol burial occurred during colder phases. High-sediment-supply during the Last Glacial Maximum hindered pedogenesis and led to the accumulation of 3-10 m-thick overbank strata. Widespread soil development (paleosol PH) occurred at the end of Last Glacial Maximum, following glaciers retreat and afforestation of drainage basins. At distal locations, paleosol PH was progressively buried under estuarine sediments during the Holocene phases of post-glacial sea-level rise. Beyond the area of marine influence, burial ages of paleosol PH change from a place to another without specific spatial trends and reflect upstream fluvial sedimentation dominated by avulsions and deposition of spatially restricted alluvial units. Holocene (H) paleosols show a poor correlation potential and laterally variable degree of maturity that reflect avulsive sedimentation patterns and crevassing. Deforestation and land reclamation affected pedo-sedimentary processes during the last 6 kyr.
Suggested Reviewers:	Timothy Demko University of Minnesota tdemko@d.umn.edu
	Mary Kraus University of Colorado Mary.Kraus@colorado.edu
	Chiara Zuffetti La Statale: Universita degli Studi di Milano

chiara.zuffetti@unimi.it

Kyungsik Choi
Seul National University
tidalchoi@snu.ac.kr; tidalchoi@hotmail.com; kschoi@kis.kigam.re.kr

Stephen Hasiotis
University of Kansas
hasiotis@ku.edu

Dear Editor,

please find enclosed the research paper "**Timing and mechanisms of sediment accumulation and pedogenesis. Insights from the Po Plain (Northern Italy)**" by Bruno L., Campo B., Hajdas I., Hong W., Amorosi A. that we would like to submit for publication in your journal *Palaeo 3*.

The manuscript has been prepared in accordance with the authors guidelines.

Best regards,

Dr. Luigi Bruno

The details of the corresponding author are as follows:

Dr Luigi Bruno

Department of Chemical and Geological Sciences

University of Modena and Reggio Emilia

Via Campi 103, 41125, Modena, Italy

E-mail: luigi.bruno@unimore.it

1   **Highlights**

2

3   • Po Plain pedostratigraphy reveals relations between pedogenetic and alluvial events

4

5   • Upper Pleistocene-Holocene stacked paleosols testify to intermittent pedogenesis

6

7   • Radiocarbon dates permitted to estimate the duration of the main pedogenetic phases

8

9   • Climate change and eustasy controlled Late Pleistocene pedo-sedimentary evolution

10

11   • Discontinuous Holocene paleosols reflect avulsive sedimentation and crevassing

1 **Timing and mechanisms of sediment accumulation and pedogenesis: insights from the Po Plain**

2 **(Northern Italy)**

3

4

5 Luigi Bruno

6 *Department of Chemical and Geological Sciences, University of Modena and Reggio Emilia, Via Campi 103,*

7 *Modena, Italy, luigi.bruno@unimore.it (corresponding author).*

8

9 Bruno Campo

10 *Department of Biological, Geological and Environmental Sciences, University of Bologna, Via Zamboni 67,*

11 *Bologna, Italy.*

12

13 Irka Hajdas

14 *Laboratory of Ion Beam Physics, ETH, Schafmattstrasse 20, 8093 Zurich, Switzerland.*

15

16 Wan Hong

17 *KIGAM Korea Institute of Geoscience and Mineral Resources, 92 Gwahangro, Yuseong-gu, Daejeon*

18 *Metropolitan City, Korea.*

19

20 Alessandro Amorosi

21 *Department of Biological, Geological and Environmental Sciences, University of Bologna, Via Zamboni 67,*

22 *Bologna, Italy.*

23

24

25

Abstract

Paleosol stratigraphy in the Po Plain, reconstructed through sedimentological analysis and correlation of ca. 170 core data chronologically constrained by 376 radiocarbon dates, revealed strict relationships between pedogenetic and fluvial processes in alluvial and paralic environments. Vertically stacked, weakly developed paleosols within Upper Pleistocene and Holocene mud-prone strata testify to intermittent pedogenesis, periodically interrupted by overbank sedimentation. Individual paleosols are laterally traceable for tens of km and exhibit A-Bk-Bw, A-Bk or A-Bw profiles. Stratigraphically ordered ^{14}C calibrated ages from A horizons testify to slow aggradation during 4-6 thousand years-long exposure periods. Burial ages, with an error of few centuries, are provided by plant debris at the top of A horizons.

Millennial-scale climate oscillations and glacio-eustasy are the main drivers of the pedo-sedimentary evolution of the area during the last 50 kyr. Pleistocene (P) paleosols developed in well-drained floodplain environments, dissected by fluvial incision, during relatively warm periods. Overbank sedimentation and paleosol burial occurred during colder phases. High-sediment-supply during the Last Glacial Maximum hindered pedogenesis and led to the accumulation of 3-10 m-thick overbank strata. Widespread soil development (paleosol PH) occurred at the end of Last Glacial Maximum, following glaciers retreat and afforestation of drainage basins. At distal locations, paleosol PH was progressively buried under estuarine sediments during the Holocene phases of post-glacial sea-level rise. Beyond the area of marine influence, burial ages of paleosol PH change from a place to another without specific spatial trends and reflect upstream fluvial sedimentation dominated by avulsions and deposition of spatially restricted alluvial units. Holocene (H) paleosols show a poor correlation potential and laterally variable degree of maturity that reflect avulsive

49   sedimentation patterns and crevassing. Deforestation and land reclamation affected pedo-

50   sedimentary processes during the last 6 kyr.

51

52

53   **Keywords**

54   Paleosol stratigraphy, pedo-sedimentary evolution, radiocarbon dates, climate change, eustasy,

55   Late Quaternary

56

57

58   1. INTRO

59

60   In alluvial settings, the development and burial of soil horizons are intimately related to fluvial

61   activity (Kraus and Bown, 1993) and governed by a variety of factors. High sediment supply and

62   fluvial aggradation inhibit pedogenesis (Demko et al., 2004), whereas low sediment supply and

63   fluvial incision promote soil development in interfluvial areas (Blum and Törnqvist, 2000). Climate

64   influences the amount of sediment delivered to the basins, modulating the magnitude and type of

65   precipitations, the vegetation cover of drainage areas and the river's transport capacity

66   (Vandenberghe, 2003). Alluvial sedimentation can be locally hindered or enhanced by tectonic

67   movements (Holbrook and Schumm, 1999; Viseras et al., 2003; Benvenuti et al., 2008; Pati et al.,

68   2019), differential subsidence (Cohen et al., 2003) or by avulsions and other processes related to

69   the intrinsic dynamics of the fluvial apparatus (Kraus, 1999; Cleveland et al., 2007; Hajek and

70   Wolinsky, 2012). In coastal settings, fluvial dynamics are strongly influenced by sea-level oscillations

71   (Atchley et al., 2004; Blum et al., 2013). Incised valleys (and associated interfluve paleosols) related

72   to glacio-eustasy are a widely recognized trait in the sedimentary record (Shanley and McCabe,

73   1994; Aitken and Flint, 1996; McCarthy and Plint, 1998; Plint et al., 2001; Gibling et al., 2011).

74   The causal relationships between paleosol formation and alluvial sedimentation have been

75   reconstructed in ancient alluvial successions, where the geometric relationships between paleosols

76   and associated fluvial sediment bodies are superbly exposed (Gibling and Bird, 1994; McCarthy and

77   Plint, 2003; Dubiel and Hasiotis, 2011; Soares et al., 2020). However, the role of distinct controlling

78   factors on paleosol development and burial can hardly be assessed (Wright and Marriott, 1993;

79   Atchley et al., 2004), because of the temporal resolution of pre-Quaternary dating methods,

80   insufficient to describe pedo-sedimentary processes which typically act at millennial time scales

81   (Rasbury et al., 1997; Hofmann et al., 2017). Furthermore, diagenesis may have substantially

82   modified soil properties after burial, hindering comparison with modern soils and the reconstruction

83   of the soil-forming environment (Trendell et al., 2012).

84   Improved techniques of subsurface investigation have recently prompted the study of buried

85   upper Quaternary alluvial successions (Choi, 2005; Tsatskin et al., 2015; Amorosi et al., 2017a,b). In

86   this relatively narrow time window, drainage areas, ecosystems and soil-forming environment did

87   not change significantly. Moreover, the high temporal resolution of Quaternary dating methods

88   permits to link unequivocally pedogenetic processes to a well-known climate and eustatic history.

89   Radiocarbon is probably the most reliable dating method for the last 50 kyr (Reimer et al., 2020).

90   However, numerous uncertainties remain in the interpretation of ^{14}C dates from paleosols. Organic

91   carbon is continuously incorporated in soils, and subjected to complex, and not totally understood,

92   biological and physical transformations (Larionova et al., 2017; Meingast et al., 2020). These

93   processes can act at different velocity and magnitude, depending on climate, morphology of the

94   exposed surface, parent material, and vegetation (Alexandrovskiy and Chichagova, 1998; Kleber,

95   2010).

96 This study is based on refined pedostratigraphic reconstructions and on a vast ^{14}C dataset which

97 permitted to chronologically constrain the major architectural and facies changes. The primary aim

98 of this research is to understand the causes and mechanisms of soil development and burial in an

99 alluvial-deltaic setting and its relation to fluvial and coastal dynamics. To this purpose, we focused

100 on Upper Pleistocene-Holocene paleosols and on their stratigraphic relationship with older, coeval

101 and younger pedo-sedimentary units. Secondary objectives are to discuss: (i) the relative role of

102 global and local controlling factors on soil development and burial; (ii) the potential use (and major

103 limitations) of radiocarbon to assess the exposure age of paleosols.

104

105

106 **2. GEOLOGICAL SETTING**

107

108 **2.1. Structural setting and basin-scale stratigraphy**

109

110 The Po sedimentary basin is enclosed in a natural amphitheatre bordered by the Alps, to west

111 and to the north, and by the Apennines, to the south. The eastward prolongation of the Po Plain is

112 the Adriatic epicontinental sea (Fig. 1). The most external thrusts of the Southern Alps and of

113 Apennines, showing opposite vergence, locally face each other beneath the Po Plain (Fantoni et al.,

114 2004). South-Alpine buried thrusts are arranged in a single wide arc running from Milan to the Garda

115 Lake (Vannoli et al., 2015). The Apennine front is composed of three tectonically active arcuate

116 thrust systems: from west to east, the Monferrato, Emilia and Ferrara-Romagna Arcs (Ghielmi et al.,

117 2013). Thrusts of the Emilia and Ferrara Arcs are sealed beneath a pile of sediments with extremely

118 variable thicknesses (from a few hundred metres to ca. 8 km; Amadori et al., 2019). These lateral

119 variations in thickness are controlled by lateral changes in subsidence rates (Campo et al., 2020),

ranging between zero and 2 mm/ (Bruno et al., 2020a). The northern margin of the Apennines, which corresponds to an out-of-sequence system of N-NE verging thrusts (Maestrelli et al., 2018), has been involved in a generalized uplift since the Early Pleistocene (Argnani et al., 2003).

The Po Basin fill shows and overall regressive trend from deep-marine to continental and coastal units (Ghielmi et al., 2013). Widespread alluvial sedimentation started in the Po Plain around 870 kyr B.P. (Muttoni et al., 2003, 2011; Gunderson et al., 2014). The Po River, flowing in W-E direction, divides the alluvial plain in two sectors (Fig. 1A). In the norther sector, Alpine tributaries flow entrenched in Pleistocene sandy units (Ravazzi et al., 2012; Fontana et al., 2014; Bruno et al., 2018). To the south, paleosol-bearing Pleistocene muds are sealed by a thick (up to 30 m) Holocene alluvial and paralic succession (Amorosi et al., 2017a, b). Early Holocene estuarine deposits typically onlap onto Upper Pleistocene alluvial strata, testifying to the progressive drowning of the alluvial plain after 11.5 cal kyr B.P. (Bruno et al., 2017). Following stabilization of sea-level, the Middle-Late Holocene records the progressive filling of the Po estuary and the successive delta progradation (Amorosi et al., 2017b, 2019).

2.2.   Paleosols of the Po Basin

Highly weathered rubified soils have been reported from the Po Basin margin (Cremaschi, 1987; Garzanti et al., 2011) and from isolated hills in the alluvial plain, generated by South-Alpine (Zerboni et al., 2015) and Apennine blind thrusts (Zuffetti et al., 2018). In depocentral areas, mature paleosols are replaced by sequences of aggradationally stacked, weakly developed paleosols laterally traceable for tens of km (Amorosi et al., 2017a). A series of closely spaced paleosols, marking the MIS 3/MIS 2 transition, has been described as the equivalent of the Interfluve Sequence Boundary (McCarty and Plint, 2003) in a high accommodation setting, due to its peculiar geometric

144 relationships with genetically related fluvial-channel bodies (Amorosi et al., 2017a). The most

145 widespread paleosol reported in the Po Plain marks the Pleistocene-Holocene boundary and

146 responds to several local names: 'Caranto' in the Venetian Plain (Mozzi et al., 2003), 'Ringhiera

147 paleosol' in the Romagna area (Ravazzi et al., 2006), 'YD paleosol' in the Po Delta Plain (Amorosi et

148 al., 2017b; Morelli et al., 2017), 'PH paleosol' in the Bologna urban area (Amorosi et al., 2014; Bruno

149 et al., 2020b; this name will be used in this paper). Although a wide literature reported the existence

150 of this pedogenized horizon, the mechanisms and causes of its formation and burial are not yet fully

151 understood. More discontinuous paleosols have been described from the Holocene succession

152 (Bruno et al., 2015, 2013).

153

154

155 **3. METHODS**

156

157   This work is based on the sedimentological and stratigraphic analysis of core material. Sixty-nine

158 cores, 30-50 m deep (red circles in Fig. 2), were analysed and sampled for radiocarbon dating. For

159 each core lithology, grainsize, colour and accessory materials (vegetal and shell macrofossils,

160 carbonate concretions, redoximorphic features) were reported. The reaction to HCl was tested as a

161 qualitative indicator of the presence of calcium carbonate. Resistance was measured on fine-grained

162 sediments with a Pocket Penetrometer (PP). One hundred and seventy-two wood, peat, vegetal-

163 remains and bulk-soil samples were dated at the KIGAM AMS laboratory (Daejeon, Republic of

164 Korea) and at the Ion Beam Physics laboratory of the ETH (Zurich, Switzerland, Synal et al., 2007).

165 Samples were collected fresh from the innermost part of the core and desiccated in a 40° oven. The

166 humin fraction was separated through acid-alkali-acid (AAA) pre-treatment and AMS dated. Humic

167   acids, extracted from 9 bulk soil samples were also dated. Conventional ^{14}C ages were calibrated

168   using OxCal 4.4, with the IntCal 20 curve (Reimer et al., 2020).

169   More than 100 core descriptions from previous works and from the database of the Geological,

170   Seismic and Soil survey of Regione Emilia-Romagna (yellow circles in Fig. 2) were reinterpreted

171   following calibration with new cores. These descriptions provide information on lithology, colour,

172   consistency, reaction to 10% HCl, pocket penetrometer measurement and radiocarbon dates.

173   Additional 204 radiocarbon dates derive from previously published works (Geological Map of Italy

174   to scale 1:50.000; Ravazzi et. al., 2006; Cacciari et al., 2017; Marabini and Vai, 2020).

175

176

177   **4. RESULTS**

178

179   **4.1. Sedimentary facies**

180

181   The sedimentological analysis of the studied cores led to the identification of several facies

182   associations which belong to alluvial, deltaic, estuarine and shallow-marine depositional

183   environments. To the purposes of this paper, we will describe in detail four main facies associations,

184   which are part of the alluvial, upper delta-plain and inner estuary depositional systems. For other

185   facies associations, the reader is referred to Amorosi et al. (2017b, 2019) and Bruno et al. (2017).

186

187   4.1.1. Fluvial channel-related facies association (FCR)

188

189   This facies association is composed of cross-stratified or laminated coarse-to-fine sand with local

190   mud intercalations (Fig. 3). The occasional presence of floated woods or plant debris is recorded.

191   Marine or lagoonal macrofossils are absents, whereas shell fragments of freshwater gasteropods

192   are seldom encountered.

193   Based on lithology, sedimentary structures and on the lack of marine and lagoonal macrofossil,

194   these coarse-grained deposits are interpreted as related to fluvial activity (in-channel deposition,

195   bar migration, crevassing, proximal overbank; Miall, 1985; Toonen et al., 2012; Aslan, 2013).

196

197   4.1.2. Freshwater swamp and marsh (SM)

198

199   This facies association is dominated by fine-grained material, with abundant wood, vegetal

200   remains and peat (Fig. 3). Peat horizons, 5-30 cm thick, are composed of poorly decomposed woody

201   material and are separated by grey (2.5 YR 7.1, 7.5 YR 8/1), peat-free clays. Freshwater fossils were

202   locally encountered. Consistency is very weak and PP values are < 1 kg/cm^2. Carbonate concretions

203   and redoximorphic features are absent. This facies association shows poor lateral extent in the

204   Upper Pleistocene succession. On the contrary, in Holocene distal deposits it is volumetrically

205   dominant and only locally interrupted by channel-related sands.

206   The grainsize of this facies group denotes a low-energy depositional environment. The

207   abundance of poorly decomposed organic material and the lack of oxidation suggest the setting of

208   reducing conditions in submerged environments. The latter were likely isolated ponds during the

209   Late Pleistocene, and swamp-marshes part of wider delta-plain and bayhead delta systems during

210   the Holocene (Amorosi et al., 2017b; Bruno et al., 2017; Cacciari et al., 2020). Peat horizons

211   separated by peat-free clays testify to intermittent sedimentation, with peat accumulation during

212   sedimentation breaks (Hijma and Cohen, 2011; Ishii et al., 2016; Bruno et al., 2019).

213

214   4.1.3. Poorly drained floodplain (PDFP)

215

216   This facies association is composed of grey (7.5 YR 6/1) silty clays with faint lamination given by

217   millimetre-scale silt intercalations. Soft and isolated carbonate concretions (CC in Fig. 4) and sparse

218   plant debris (UOM in Fig. 4) were seldom encountered. Redoximorphic features are lacking.

219   Freshwater gasteropods were seldom encountered. Consistency is weak to firm. Pocket

220   penetrometer values are in the range of 1-2 kg/cm^2.

221   Based on grainsize and fossil content, this facies association is interpreted as deposited in a distal

222   fluvial environment, occasionally subjected to river flooding. Lack of redoximorphic features

223   suggests a groundwater table fluctuating close to the topographic surface (poorly drained

224   floodplain). The amount, distribution and type of secondary calcite are consistent with this

225   interpretation.

226

227   4.1.4.   Well-drained floodplain (WDFP)

228

229   This facies association is composed of firm-to-hard clayey silts and silty clays. Sedimentary

230   structures are absent. By contrast, polygonal structures, desiccation cracks and rootlets are

231   commonly observed. A well-expressed horizonation is given by colour and CaCO$_3$ distribution (Fig.

232   3). Dark horizons, showing weak or no reaction to HCl alternate with lighter horizons showing strong

233   reaction to HCl. Carbonate concretions, in the form of coalescent nodules, coatings, filaments and

234   sub-horizontal bands are observed in lighter horizons. Redoximorphic features, in the form of

235   orange mottles or bands (RF in Fig. 6), are commonly observed at the mesoscale. Plant debris and

236   freshwater gasteropods are seldom encountered. PP values are > 2 kg/cm^2.

237   As for facies PDFP, grainsize and fossil content point to a distal fluvial environment, occasionally

238   inundated by river waters (Collinson, 1996). The alternation of dark and light horizons is interpreted

239   as the result of multiple phases of soil development interrupted by overbank deposition and

240   paleosol burial. Dark colour reflects the accumulation and decomposition of organic matter in the

241   topsoil (Bruno et al., 2020b). Carbonate distribution, with carbonate-free horizons overlying $CaCO_3$

242   enriched horizons, is interpreted as the result of carbonate leaching from the topsoil (A horizon)

243   and illuviation to the underlying Bk horizon (Boul et al., 2011). Carbonate mobilization requires the

244   percolation of meteoric waters in a vadose zone. We, thus, argue that the groundwater was located

245   a few metres below the topographic surface during subaerial exposure (well-drained floodplain).

246

247

248   **4.2.   Paleosol stratigraphy**

249

250   Paleosols were identified at three stratigraphic intervals in the Upper Pleistocene-Holocene

251   succession of the Po Plain.

252   The lower interval is composed of a series of closely-spaced paleosols (paleosols P in Figs. 4, 5

253   and 6), whose cumulative thickness is in general < 5 m. Calibrated ages span from the ^{14}C detection

254   limit (~50 kyr B.P.) to ~23 kyr B.P. (Figs. 5 and 6). These paleosols show A-Bk-Bw or A-Bk profiles. A

255   horizons, 30-50 cm thick, are decalcified (Bruno et al., 2020b; Amorosi et al., this volume) and

256   present diffuse organic matter (DOM in Fig. 4) and slight bands of Fe oxides and/or hydroxides (Fig.

257   3). Undecomposed organic matter was not observed and carbonate concretions have locally been

258   reported from the base and the top of these horizons. Bk horizons are typified by high $CaCO_3$ content

259   (30-40% of the total volume, Bruno et al., 2020b). Carbonate concretions are abundant as

260   coalescent nodules or whitish sub-horizontal bands (evolutionary stage II of Gile et al., 1981;

261   Machette, 1985). Transition to overlying and underlying horizons is in general gradational. Bw

262   horizons show moderate $CaCO_3$ content (Bruno et al., 2020b; Amorosi et al., this volume) and faint

mottles of Fe oxides and-or hydroxides. Evidences of clays mobilization (Bt horizons) were not

observed. At distal locations, these paleosols may show less clear horizonation (A-Bw profile) or may

be replaced by coeval peat-bearing swamp deposits (Fig. 5).

In the second interval, a single paleosol (paleosol PH, Figs. 4, 5 and 6) is encountered at the top

of a 3-10 m thick sedimentary unit composed of overbank muds and subordinated channel-related

sands (Last Glacial Maximum Sedimentary Unit, LGM SU in Figs. 4, 5 and 6). Textural characters of

paleosol PH vary from proximal to distal locations. At inland locations (core EM15, Fig. 3), paleosol

PH shares many characteristics with older P paleosols: (i) a carbonate-free, brown (10YR 4/4, 3/3) A

horizon, up to 100 cm thick, with DOM and RF; (ii) a lighter Bk horizon with abundant nodules or

bands of secondary calcite (evolutionary stage II); (iii) a Bw horizon showing evidence of incipient

alteration. At more distal locations (cores EM1 and EM3, Fig. 3), paleosol PH exhibit a grey (5Y 4/1,

2.5Y 6/1) decalcified A horizon, 30-50 cm thick, with DOM. Plant debris, absent in the lower part,

become increasingly abundant upsection and, at places, grade into the overlying peats (see core B3,

Fig. 4). The underlying Bk horizon, when present, is relatively thin (a few dm), with secondary calcite

in the form of nodules, coatings or filaments (evolutionary stages I and II). Redoximorphic features

were not observed at the mesoscale along the whole soil profile.

In the third interval, dated to the Holocene, paleosols (H1 and H2 in Figs. 4, 5 and 6) have been

observed only at inland locations. At distal locations, they are replaced by coeval estuarine and

deltaic deposits. H paleosols have poor correlation potential and their textural features vary

dramatically from a place to another, without specific spatial trends. In few localities, they show

characteristics similar to those of their Pleistocene counterparts. At places, they are barely

identifiable due to a poorly developed horizonation. Archeological artifacts are increasingly

abundant in younger paleosols.

286   Paleosols P and PH bound nearly tabular sediment packages and are locally replaced by coeval

287   incisions filled with FCR or SM deposits (see cores CNT, RN3 and EM2, Fig. 5). On the contrary,

288   Holocene paleosols overlie or are overlain by CR facies (see cores MW and 15, Figs. 5 and 6). Alluvial

289   units delimited by these soil horizons are poorly extended and typically wedge out laterally or

290   downdip (Figs. 5 and 6).

291

292

293   **4.3.   Radiocarbon dating of paleosols**

294

295   Upper Quaternary successions provide the great opportunity to link pedo-sedimentary events to

296   the detailed climatic and eustatic history described in a vast literature (eg. Clark and Huybers, 2009;

297   Lambeck et al., 2011; Rasmussen et al., 2014). Assessing the timing of soil development and burial

298   is crucial to disentangle the relative influence of global and local factors. This chapter summarizes

299   observations deriving from the analysis of a chronological database composed of 376 radiocarbon

300   dates (160 from paleosols).

301   Along single cores, multiple dating of A horizons yielded stratigraphically ordered ages, spanning

302   3-5 kyr (see cores B3, RW28 and 13, Figs. 4, 5C and 6). Only in core SPR (Fig. 5C) two samples from

303   the base and the top of the same A horizon provided similar ages. In distal cores, plant debris from

304   topmost A horizons yielded ages that are considerably younger (up to 5 kyr) than those from bulk-

305   soil samples and just a few centuries older than those from overlying SM peats (see cores EM1, EM3

306   and B3, Figs. 3, 4 and 5). Dates from A horizons indicate aggradation at extremely low rates (0,05-

307   0,23 mm yr-1) during soil development. Accumulation rates above or between paleosols are at least

308   one order of magnitude grater (> 1 mm/yr).   Distinct ages were also obtained from different

fractions extracted from the same sample. Particularly, humic acids yielded, in 9 cases out of 10, ages older than those obtained from the humin fraction (Table 1).

Dates from bulk-soil samples change also laterally, along the same paleosol, spanning in a range of 4-6 kyr (Fig. 3). No specific trend was observed from proximal to distal locations. Ages also change over short distances, as observed in the Bologna area. In the Two Tower Medieval district, where distance between cores is just 10-20 m, six samples from paleosol P3 yielded ages in the range of 3-4 kyr (Fig. 6).

The frequency distribution of radiocarbon dates from paleosols (grey rectangles in Fig. 7) shows a major peak between 14 and 10 kyr B.P., related to the PH paleosol. Samples from the P paleosols yielded ages clustered around three minor peaks (P1, P2 and P3, Fig. 7), at 46-41, 38-32 and 29-25 cal kyr B.P., respectively. The overall decay with time in the number of ^{14}C dates across the Pleistocene simply reflects the fact that older sediments were penetrated by a progressively lower number of cores. A decline in the number of ^{14}C dates from soil samples is also recorded towards younger ages, together with a sharp increase in dates from SM and PDFP deposits. Ages from Holocene soil samples are clustered around two peaks. The older peak reflects, in part, the youngest ages from paleosol PH and in part dates from a distinct paleosol (H1 in Figs 4, 5 and 6) observed at several inland locations. In the Bubano Quarry (BQ in Fig. 5C), 5 m-thick overbank strata separate H1 from PH. In the Bologna area (core 16, Figs. 4 and 6), paleosol H1 bears Neolithic and Eneolithic artefacts (Bruno et al., 2013). The second peak (H2, Fig. 7) corresponds to another archeological level, rich in Late Bronze Age, Iron-Age and Roman rests (IR paleosol of Bruno et al., 2013), which was buried in large part of the Po Plain during the Middle Ages (see core CRV, Fig. 5A). Locally, this paleosol is still exposed (Fig. 5). Interestingly, the maximum number of ^{14}C dates from facies FCR is recorded between H2 and H1.

333

5. DISCUSSION

335

5.1 Use and limitations of radiocarbon for the estimation of the exposure age of paleosols

337

The use and reliability of radiocarbon dates from paleosols have been widely debated because, unlike plant macrofossils, which preserve the particular ^{14}C content of the moment of grow, soils are open systems where organic carbon is continuously incorporated, humified and-or oxidized to CO_2 before burial (Orlova and Panychev, 1993; Martin and Johnson, 1995; Gaudinski et al., 2000). Therefore, ^{14}C ages from paleosols reflect the mean residence time of the organic carbon plus the time of burial (Matthews, 1980; Geyh et al., 1983). The amount of organic carbon added to a soil and the velocity of its transformation processes change from place to place as a function of climate, vegetation and parent material (Reimer et al., 2020). Moreover, turnover and breakdown of organic matter may lead to the redistribution of ^{14}C ratios in different soil fractions. As a result, apparently conflicting ages can be obtained from the same paleosol (Figs. 5 and 6) and from different soil fractions (Table 1). Because of this inherent variability, many authors concluded that radiocarbon dates from soils are unreliable and the concept of "age" cannot be strictly applied to paleosols (Gilet-Blein et al., 1980; Becker-Heidmann et al., 2002). However, if not subjected to post-burial contamination (e.g. rootlets), paleosols should yield ages scattered within its formation period. The estimation of the length of this period, which can attain several millennia, is an intriguing goal for Quaternary paleosol stratigraphers.

The lack of evidence of clay mobilization, the evolutionary stage of secondary calcite and the limited rubefaction suggest that Po Plain paleosols evolved over relatively short periods. Radiocarbon ages from deposits below and above paleosols constrain their exposure period within

357 10-12 thousand years (Figs. 5 and 6). Dates from paleosols are within the narrower range of 4-6

358 millennia and provide a robust constrain for stratigraphic correlations over long distances (Amorosi

359 et al., 2017a). More complex is the precise assessment of the ages that mark the onset and end of

360 pedogenesis for each paleosol, even if radiocarbon dates are available from the base and top of A

361 horizons. Previous work has demonstrated that, although some organic carbon can remain in soils

362 for millennia (Feng, 2009), the oldest organic fraction accumulated at the onset of pedogenesis may

363 have been completely replaced by younger organic carbon (Scharpenseel, 1971; Alexandrovskiy and

364 Chichagova, 1998) introduced by roots in the deepest soil horizons. Thereby, radiocarbon dates

365 from organic-sediment samples collected from the base of the A horizon may not be representative

366 of the onset of soil formation (Gilet-Blein et al., 1980; Alexandrovskiy and Chichagova, 1998). Several

367 factors influence carbon turnover times in soils (Kleber, 2010; Chen et al., 2013; Pandey et al., 2014).

368 Particularly, carbon renewal is slower in colder climates and in deep soil horizons (Alexandrovskiy

369 and Chichagova, 1998; Gaudinski et al., 2000; Fontaine et al., 2007). Therefore, for soils that

370 developed in cold climatic conditions, such as paleosols P3, which formed at the onset of Last Glacial

371 Maximum, dates from the base of the A horizon should better approximate the onset of

372 pedogenesis. This assumption is corroborated by dates from core B3 (Figs. 3, 4 and 5), where the

373 oldest age from paleosols P3 partially overlaps the age from underlying paleosol P2. For paleosols

374 developed in warmer periods (PH and H paleosols), ages from the base of A horizons may post-date

375 the onset of pedogenesis.

376   Sediment samples collected from the top of A horizons may be older than burial time, because a

377 certain amount of time is required for litter humification and mineralization (Chichagova and

378 Cherkinsky, 1993). At inland locations of our study area, where O horizons are generally not

379 preserved, burial ages cannot be assessed precisely. Available dates permit to assert, for example,

380 that paleosol PH was buried after 10.3 kyr B.P. in core 13 (Figs. 4 and 6) and between 14.3 and 8.6

381   kyr B.P. in core 201S4 (Fig. 5). Conversely, at distal locations, plant macrofossils preserved in the

382   topsoil provides ages that approximate the paleosol burial age with an error of a few centuries. For

383   example, in EM1, where estuarine sedimentation was already established around 8.1 kyr B.P., burial

384   of paleosol PH occurred around 8.5 kyr B.P. (Figs. 3, 4 and 5).

385   Age/depth gradients, like those observed in the Po Plain paleosols, have been reported from

386   several soil profiles (Matthews, 1981; Matthews and Dresser, 1983; Alexandrovskiy and Chichagova,

387   1998; Becker-Heidmann et al., 2002) and can possibly be explained by the fact that the amount of

388   carbon added to the topsoil through litter accumulation is in general order of magnitudes greater

389   than the one introduced in deeper soil horizons via roots exudation (Fontaine et al., 2007). The

390   measured accumulation rates, incompatible with alluvial sedimentation, suggest that litter

391   accumulation accounted for soil aggradation during exposure, with a possible contribution of wind-

392   transported dust. Therefore, paleosols from the Po Plain represent condensation horizons, rather

393   than depositional hiatuses. On the contrary, sedimentation between pedogenetic phases seems a

394   quasi-instantaneous process (see ages from P2 and P3 in core B3, Figs 4 and 5). Paleosols

395   aggradation is also testified by the presence of carbonate concretions in lower A horizons, likely

396   related to the upward migration of the eluvial-illuvial (A-B) boundary, and by vertically stacked sub-

397   horizontal bands of secondary calcite in Bk horizons (Fig. 3). Carbonate concretions in upper A

398   horizons, on the other hand, reflect post-burial illuviation from overlying paleosols. For this reason,

399   we avoided radiocarbon dating of carbonates and removed secondary calcite in acid steps of the

400   AAA sample preparation, before AMS analysis. Humic acids are also considered as a mobile

401   compound, which may yield anomalously young ages due to contamination from overlying strata

402   (Matthews, 1980). In our case, the oldest ages are provided by humic acids (Table 1). We thus

403   excluded contamination from overlying strata during each phase of pedogenesis.

404

5.2. Pedo-sedimentary evolution of the Po Plain and controlling factors

With the chronological constraint of 376 radiocarbon dates, the alluvial succession of the southern Po Plain provides an unprecedent record of pedo-sedimentary events across the last 50 kyr.

Aggradationally stacked paleosols 'P' developed during the Late Pleistocene, when the Adriatic coastline migrated in response to the stepwise sea-level fall toward its lowstand position, ~300 km away from the modern one (Pellegrini et al., 2018). Among P paleosols, only P3 developed during a phase of sea-level drop (~30–50m between 30 and 24 cal ka BP, Peltier and Fairbanks, 2006; Fig. 7B). Conversely, P1 and P2 developed in a period characterized by low-amplitude sea-level oscillations (Chappell, 2002; Fig. 7B). Far from the influence of sea-level change, pedo-alluvial processes are controlled by the balance between sediment supply and water discharge (Blum and Törnqvist, 2000). Low sediment supply-discharge ratios result in channel incision and soil development in the adjacent interfluves, whereas high sediment supply-discharge ratios promote fluvial aggradation and paleosol burial (Demko et al., 2004). Bruno et al. (2020b) documented that soil development and burial during the Late Pleistocene was mainly controlled by changes in vegetation driven by climatic oscillations at the scale of Bond cycles (Bond et al., 1993). Soils started to form at the onset of Bond cycles, when warm climate conditions favoured the spread of dense forests (Magri, 1999; Fletcher et al., 2010), which protected the Apennine drainage basins from erosion (low sediment supply). Soil development was systematically interrupted during the subsequent cold phases, at the culmination of Bond cycles, corresponding to North Atlantic Heinrich events (light blue vertical lines in Fig. 7B). These periods record generalized forest retreats (Fletcher et al., 2010; Helmens, 2014), which enhanced erosion in the drainage basins and sediment transfer to the alluvial plains. Increased sediment supply promoted the filling of fluvial incisions and the

burial of formerly exposed interfluves by overbank sedimentation. Thin sediment packages were deposited between two successive phases of subaerial exposure (Figs. 3 to 6). These deposits (and, partly, the underlying paleosols) were modified during the successive pedogenetic phase. A similar response to millennial-scale climate oscillations has been observed in loess paleosol-bearing successions (Rousseau et al., 2011, 2007; Moine et al., 2017; Zeeden et al., 2018).

The Last Glacial Maximum was characterized by deposition of thick and widespread fluvial-channel gravel-sand bodies in the Po Plain (Ravazzi et al., 2012; Campo et al., 2016) and in other alluvial systems worldwide (Lewis et al., 2001; Briant et al., 2005). Alpine glaciers, which extended down to the Po Plain margin, supplied huge amounts of sediments to the related fluvio-glacial systems (Fontana et al. 2014). In the Apennine domain, high sediment supply, favoured by a predominantly herbaceous vegetation cover of drainage basins (Vescovi et al., 2010), resulted in the deposition of the LGM SU, which bears poor evidence of pedogenesis (Figs. 4, 5 and 6).

Above the LGM SU, PH is the most widespread paleosol in the Po Plain. This surface yielded radiocarbon dates spanning between ~17 and 6 kyr B.P. (Fig. 8), but mostly clustered around 14 and 10 kyr B.P. (Fig.7). The precise assessment of the age of PH formation is hampered by paucity of dateable material from the underlying LGM SU. However, available dates indicate that the onset of post-LGM pedogenesis was diachronous across the Po Plain, without a specific spatial trend (Fig. 8). Whereas in the Bologna area PH started to develop at least 16.8 kyr B.P. (see core RW28, Figs 6 and 8), in the Romagna plain (Bubano Quarry - BQ, in Figs 5C and 8) pedogenesis started after 14.4 kyr B.P. (Ravazzi et al., 2006). We argue that post-LGM pedogenesis was favoured by decreased sediment supply related to the progressive afforestation of the area (Pini et al., 2010; Vescovi et al., 2010; Campo et al., 2020), with diachroneity possibly related to particular local conditions (e.g. distance from active channels). North of the Po River, in the Alpine tributary system, fluvial incision

453 occurred soon after glacial retreat (~17 kyr B.P., Monegato et al., 2017), due to sediment trapping

454 in lakes which formed in place of abandoned glacial amphitheatres (Fontana et al., 2014).

455   Interestingly most of the ^{14}C dates from paleosol PH post-date the Oldest Dryas (OD in Fig. 7).

456 The clustering of dates around the Younger Dryas in the Po delta plain (Figs. 7A and 8), suggested a

457 possible control of this cold event on paleosol formation (Amorosi et al., 2017b, Morelli et al., 2017).

458 The wider dataset shown in this work highlights that pedogenesis started in many sites of the Po

459 Plain at least during the Bølling and Allerød warm phases (BA in Fig. 7A). Unlike cold phases at the

460 culmination of pre-LGM Bond cycles, the Younger Dryas cold spell did not lead to paleosol burial.

461 This event was probably too short-lived to promote the filling of fluvial incisions and overbank

462 sedimentation. Paleosol development recorded after LGM in other alluvial (Mol, 1997; Choi, 2005;

463 van Balen et al., 2010; Janssens et al., 2012) and eolian (Kaiser et al., 2009; Hošek et al., 2017)

464 successions, indicates a likely climate control at a supra-regional spatial scale. Progressively warmer

465 conditions lead to widespread afforestation and reduced sediment supply (Fletcher et al., 2010;

466 Helmens, 2014).

467   Whereas Alpine rivers still flow entrenched in Pleistocene deposits, Apennine incisions were filled

468 during the Early Holocene (see cores RN3 and EM2, Fig. 3C) and paleosol PH was buried soon after.

469 In the coastal plain, where paleosol PH is encountered at greater depths beneath estuarine deposits,

470 burial ages show an overall inverse power law with elevation (Fig. 9) that reflects the progressive

471 drowning of the area during the early Holocene sea-level rise (Bruno et al., 2017). Slight dispersion

472 of data may reflect post-burial deformation of paleosol PH by differential subsidence and

473 neotectonics (Amorosi et al., 2021). In the area under marine influence (shades of blue in Fig. 10),

474 burial ages decrease landwards from ~11.5 to 5.4 kyr B.P.. This overall spatial trend is not recorded

475 in two isolated areas, where paleosol PH and older paleosols are upbended (see also Fig. 5C). In

476 cross-sections, the progressive drowning of paleosol PH is testified by onlap terminations of

477   Holocene flooding surfaces (Fig. 5A). These horizons, associated to prominent facies backstepping,

478   are coeval to the main Holocene melt water pulses (MWP-1b, 1c, 1d; Fig. 7B), which forced the

479   landward migration of the Po estuary across the study area. The effects of MWP-1A are not recorded

480   in the study area, which was too far from the coastline at that time (Storms et al., 2008).

481   Pedo-sedimentary features of paleosol PH reflect this evolutionary history. Carbonate

482   redistribution along the soil profile and relatively low amounts of organic carbon in the A horizons

483   (Amorosi et al., this volume) are indicative of a low groundwater table (Kalisz et al., 2010), enhanced

484   by fluvial incision during the early phases of soil development (Tebbens et al., 1999). Preserved plant

485   debris in the topsoil, radiocarbon dated to the early Holocene (Figs. 4 and 5), reflects the progressive

486   rise in groundwater table (Bohacs and Suter, 1997) up to the setting of waterlogged conditions and

487   to the accumulation of peat beds (Diessel, 1992; Richardson and Vepraskas, 2001; Stolt and

488   Rabenhorst, 2011). The rise of the groundwater table, forced by sea-level rise (Kosters and Suter,

489   1993; Törnqvist, 1993; Wadsworth et al., 2003), led to the progressive filling of Apennine fluvial

490   incisions by fine-grained and organic-matter-rich estuarine strata (facies SM, cores RN3 and EM2 in

491   Fig. 5C). The lack of fluvial sands (facies FCR) at the base of fluvial incisions, suggests that valley

492   filling was promoted by eustasy rather than by an upstream increase in sediment supply (Kvale and

493   Archer, 2007).

494   Beyond the area of marine influence, at elevations > -3 m, the burial age of paleosol PH is

495   substantially unpredictable (Figs. 9 and 10). The dispersion of burial dates in this upstream sector

496   reflects the dynamics of Holocene sedimentation, dominated by avulsion processes and by the

497   deposition of poorly extended alluvial units (Figs. 5 and 6). This aspect is particularly evident in the

498   Bologna area (Fig. 6): in core 16, for example, paleosol PH was already buried around 8.2 kyr B.P.,

499   when paleosol H1 was still developing (see also Fig. 4); in the nearby core 15, at a distance of just

500   224 m, the burial of paleosol PH occurred only around 7 kyr B.P.. The transition to an avulsive

501 sedimentation pattern at the onset of the Holocene, recorded in several worldwide fluvial systems

502 (Phillips, 2011; Stouthamer et al., 2011), is an indirect consequence of the landward migration of

503 the coastline, which dramatically reduced the area available for sediment storing and lowered rivers

504 longitudinal gradients. Decreased stream power, and capability to erode banks and create space for

505 sediment storage, led to river aggradation, crevassing and avulsions (Blum et al., 2013).

506   The discontinuity of Holocene paleosols (Figs. 5 and 6) reflects the limited areal extent of the

507 sedimentary units on which they developed. Avulsive sedimentation patterns and crevassing also

508 determined laterally variable maturity of Holocene paleosols. Indeed, soil development was

509 interrupted only in restricted areas affected by alluvial deposition. In sediment-starved areas, soils

510 continued to evolve. Lateral changes in soil maturity are observable in modern soils, which started

511 to develop during the Late Bronze age (areas where H2 is still exposed – Fig. 5), and after the Middle

512 Ages (areas where H2 is buried - Fig. 5).

513   The peak in radiocarbon dates from fluvial channel-related deposits, centred around 5-6 kyr B.P.

514 (Fig. 7), corresponds to a generalized re-organization of the river network at the onset of

515 Neoglaciation (Piovan et al., 2012; Bruno et al., 2015; Amorosi et al., 2017b), which led to the burial

516 of paleosol H1. Slope instability and enhanced sediment production, recorded in the Northern

517 Apennines since 5.5 kyr B.P. (Soldati et al., 2006; Picotti and Pazzaglia, 2008), likely reflect

518 widespread deforestation of the Apennine drainage basins during the early Eneolithic (Cremaschi

519 and Nicosia, 2012). The progressive return to stable floodplain conditions was paralleled by

520 improved techniques of land reclamation and management from the late Bronze age to late

521 Antiquity (Bruno et al., 2013).

522

523

524   **6. CONCLUSIONS**

525

Based on the sedimentological analysis and correlation of more than 170 core data, with the chronological constraint of 376 radiocarbon dates, this study provided new data on: (i) the complex relationships between pedogenetic, fluvial and costal processes in alluvial and paralic environments; (ii) the relative influence of global (i.e. climate and eustasy) and local (e.g. river avulsions) factors on soil development and burial; (ii) the use and limitations of radiocarbon to assess the exposure age of paleosols.

In the Upper Pleistocene-Holocene mud-prone succession of the Po Basin, vertically stacked, weakly developed paleosols testify to intermittent pedogenesis, periodically interrupted by overbank sedimentation. Radiocarbon analyses permitted to define the duration of the main phases of pedogenesis and to compare them to climate and eustatic curves.

Radiocarbon dates from paleosols (bulk-soil and plant-debris samples) and from underlying and overlying sedimentary units indicate exposure periods encompassing 4-6 millennia. This estimate is consistent with pedological features (e.g. type of secondary calcite, lack of illuvial clay, limited rubefaction), which denote incipient pedogenesis. Stratigraphically ordered ^{14}C calibrated ages within A horizons revealed that Po Plain paleosols are condensation horizons, which experienced slow aggradation during exposure (0,05-0,23 mm/yr) due to accumulation of plant litter, with a likely contribution of wind-transported dust.

Millennial-scale climate oscillations and glacio-eustasy concurred in driving the pedo-sedimentary evolution of the Po Plain during the Late Pleistocene. In particular, during the MIS 3, pedogenetic events were mainly controlled by changes in vegetation driven by climatic oscillations at the scale of Bond cycles. Paleosols developed in well-drained floodplain environments, dissected by fluvial incision, during relatively warm periods. Overbank sedimentation and paleosol burial

occurred during colder phases. During the Last Glacial Maximum, high-sediment-supply hindered pedogenesis and led to the accumulation of 3-10 m-thick overbank strata.

Widespread soil development (paleosol PH) occurred at the end of the Last Glacial Maximum, following glaciers retreat and afforestation of drainage basins. Burial of paleosol PH was diachronous as indicated by radiocarbon dates from vegetal remains preserved at the topsoil. At distal locations, paleosol PH was progressively drowned and buried under estuarine sediments during the Holocene phases of post-glacial sea-level rise. Beyond the area of marine influence, burial ages of paleosol PH change from a place to another without specific spatial trends, reflecting upstream fluvial sedimentation dominated by avulsions.

Holocene (H) paleosols, observed at inland locations, grade seaward into coeval estuarine and deltaic deposits. These pedogenized horizons show a poor correlation potential and laterally variable degree of maturity that reflect avulsive sedimentation patterns and widespread crevassing. Human activities (e.g. deforestation and land reclamation) became an increasingly important factor affecting pedo-sedimentary processes during the last 6 kyr.

This study highlights the potential for paleoenviromental reconstructions of upper Quaternary sedimentary successions. The pedo-stratigraphic approach adopted here, relying upon a robust chronological framework, permitted to assess the temporal and spatial scale of pedogenetic events and to discern the relative contribution of distinct controlling factors that typically act contemporaneously.

572

573

574   **REFERENCES**

575

576   Aitken, J.F., Flint, S.S., 1996. Variable expressions of interfluvial sequence boundaries in the

577   Breathitt Group (Pennsylvanian), eastern Kentucky, USA. Geol. Soc. London, Spec. Publ. 104,

578   193–206.

579   Alexandrovskiy, A.L., Chichagova, O.A., 1998. Age of humic substances in paleosols. Radiocarbon

580   40, 991–997.

581   Amadori, C., Toscani, G., Di Giulio, A., Maesano, F.E., D'Ambrogi, C., Ghielmi, M., Fantoni, R., 2019.

582   From cylindrical to non-cylindrical foreland basin: Pliocene–Pleistocene evolution of the Po

583   Plain–Northern Adriatic basin (Italy). Basin Res. 991–1015. https://doi.org/10.1111/bre.12369

584   Amorosi, A., Bruno, L., Rossi, V., Severi, P., Hajdas, I., 2014. Paleosol architecture of a late

585   Quaternary basin – margin sequence and its implications for high-resolution , non-marine

586   sequence stratigraphy. Glob. Planet. Change 112, 12–25.

587   https://doi.org/10.1016/j.gloplacha.2013.10.007

588   Amorosi, A., Bruno, L., Cleveland, D.M., Morelli, A., Hong, W., 2017a. Paleosols and associated

589   channel-belt sand bodies from a continuously subsiding late quaternary system (Po basin,

590   Italy): New insights into continental sequence stratigraphy. Bull. Geol. Soc. Am. 129, 449–463.

591   https://doi.org/10.1130/B31575.1

592   Amorosi, A., Bruno, L., Campo, B., Morelli, A., Rossi, V., Scarponi, D., Hong, W., Bohacs, K.M.,

593   Drexler, T.M., 2017b. Global sea-level control on local parasequence architecture from the

594   Holocene record of the Po Plain, Italy. Mar. Pet. Geol. 87, 99–111.

595   https://doi.org/10.1016/j.marpetgeo.2017.01.020

596   Amorosi, A., Barbieri, G., Bruno, L., Campo, B., Drexler, T.M., Hong, W., Rossi, V., Sammartino, I.,

597   Scarponi, D., Vaiani, S.C., 2019. Three-fold nature of coastal progradation during the

598   Holocene eustatic highstand, Po Plain, Italy–close correspondence of stratal character with

599   distribution patterns. Sedimentology 66, 3029–3052.

600   Amorosi, A., Bruno, L., Campo, B., Costagli, B., Hong, W., Picotti, V., Vaiani, S.C., 2021. Deformation

601   patterns of upper Quaternary strata and their relation to active tectonics, Po Basin, Italy.

602   Sedimentology 68, 402–424. https://doi.org/10.1111/sed.12784

603   Amorosi, A., Bruno, L., Campo, B., Di Martino, A., I. Sammartino. Patterns of geochemical variability

604   across weakly developed paleosol profiles and their role as regional stratigraphic markers (Late

605   Pleistocene, Po Plain). Submitted to this volume.

606   Argnani, A., Barbacini, G., Bernini, M., Camurri, F., Ghielmi, M., Papani, G., Rizzini, F., Rogledi, S.,

607   Torelli, L., 2003. Gravity tectonics driven by Quaternary uplift in the Northern Apennines:

608   Insights from the La Spezia-Reggio Emilia geo-transect. Quat. Int. 101–102, 13–26.

609   https://doi.org/10.1016/S1040-6182(02)00088-5

610   Aslan, A., 2013. Sediments. Encycl. Quat. Sci. Second Ed. 663–675. https://doi.org/10.1016/B978-

611   0-444-53643-3.00111-4

612   Atchley, S.C., Nordt, L.C., Dworkin, S.I., 2004. Eustatic control on alluvial sequence stratigraphy: A

613   possible example from the Cretaceous-Tertiary transition of the Tornillo Basin, Big Bend

614   National Park, West Texas, U.S.A. J. Sediment. Res. 74, 391–404.

615   https://doi.org/10.1306/102203740391

616   Becker-Heidmann, P., Andresen, O., Kalmar, D., Scharpenseel, H.W., Yaalon, D.H., 2002. Carbon

617   dynamics in Vertisols as revealed by high-resolution sampling. Radiocarbon 44, 63–73.

618   https://doi.org/10.1017/S0033822200064687

619   Benvenuti, M., Bonini, M., Moratti, G., Ricci, M., Tanini, C., 2008. Tectonic and climatic controls on

620 historical landscape modifications: The avulsion of the lower Cecina River (Tuscany, central

621 Italy). Geomorphology 100, 269–284. https://doi.org/10.1016/j.geomorph.2007.12.009

622 Blum, M.D., Törnqvist, T.E., 2000. Fluvial responses to climate and sea-level change: A review and

623 look forward. Sedimentology 47, 2–48. https://doi.org/10.1046/j.1365-3091.2000.00008.x

624 Blum, M., Martin, J., Milliken, K., Garvin, M., 2013. Paleovalley systems: Insights from Quaternary

625 analogs and experiments. Earth-Science Rev. 116, 128–169.

626 https://doi.org/10.1016/j.earscirev.2012.09.003

627 Bohacs, K., Suter, J., 1997. Sequence stratigraphic distribution of coaly rocks: Fundamental

628 controls and paralic examples. Am. Assoc. Pet. Geol. Bull. 81, 1612–1639.

629 https://doi.org/10.1306/7834e192-1721-11d7-8645000102c1865d

630 Bond, G., Heinrich, H., Broecker, W., Labeyrie, L., McManus, J., 1992. andrews J. Huon S., Jantschik

631 R., clasen S., Simet ch., Tedesco K., Klas M., Bonani G. Ivy S 245–249.

632 Bond, G., Broecker, W., Johnsen, S., McManus, J., Labeyrie, L., Jouzel, J., Bonanl, G., 1993. Bond

633 1993. Nature 365, 143–147.

634 Bond, G., Showers, W., Cheseby, M., Lotti, R., Almasi, P., DeMenocal, P., Priore, P., Cullen, H.,

635 Hajdas, I., Bonani, G., 1997. A pervasive millennial-scale cycle in North Atlantic Holocene and

636 glacial climates. Science (80-.). 278, 1257–1266.

637 Boul, S.W., Southard, R.J., Graham, R.C., McDaniel, P.A., 2011. Soil genesis and classification:

638 Hoboken, 6th ed. Wiley-Blackwell, Chichester. https://doi.org/10.1002/9780470960622.

639 Briant, R.M., Bateman, M.D., Coope, G.R., Gibbard, P.L., 2005. Climatic control on quaternary

640 fluvial sedimentology of a Fenland Basin river, England. Sedimentology 52, 1397–1423.

641 https://doi.org/10.1111/j.1365-3091.2005.00747.x

642 Bruno, L., Amorosi, A., Curina, R., Severi, P., Bitelli, R., 2013. Human-landscape interactions in the

643 Bologna area (northern Italy) during the mid-late Holocene, with focus on the Roman period.

644   Holocene 23, 1560–1571. https://doi.org/10.1177/0959683613499054

645   Bruno, L., Amorosi, A., Severi, P., Bartolomei, P., 2015. High-frequency depositional cycles within

646   the late Quaternary alluvial succession of Reno River (Northern Italy). Ital. J. Geosci. 134, 339–

647   354. https://doi.org/10.3301/IJG.2014.49

648   Bruno, L., Bohacs, K.M., Campo, B., Drexler, T.M., Rossi, V., Sammartino, I., Scarponi, D., Hong, W.,

649   Amorosi, A., 2017. Early Holocene transgressive palaeogeography in the Po coastal plain

650   (northern Italy). Sedimentology 64, 1792–1816. https://doi.org/10.1111/sed.12374

651   Bruno, L., Piccin, A., Sammartino, I., Amorosi, A., 2018. Decoupled geomorphic and sedimentary

652   response of Po River and its Alpine tributaries during the last glacial/post-glacial episode.

653   Geomorphology 317, 184–198. https://doi.org/10.1016/j.geomorph.2018.05.027

654   Bruno, L., Campo, B., Di Martino, A., Hong, W., Amorosi, A., 2019. Peat layer accumulation and

655   post-burial deformation during the mid-late Holocene in the Po coastal plain (Northern Italy).

656   Basin Res. 31, 621–639. https://doi.org/10.1111/bre.12339

657   Bruno, L., Campo, B., Costagli, B., Stouthamer, E., Teatini, P., Zoccarato, C., Amorosi, A., 2020a.

658   Factors controlling natural subsidence in the Po Plain. Proc. Int. Assoc. Hydrol. Sci. 382, 285–

659   290. https://doi.org/10.5194/piahs-382-285-2020

660   Bruno, L., Marchi, M., Bertolini, I., Gottardi, G., Amorosi, A., 2020b. Climate control on stacked

661   paleosols in the Pleistocene of the Po Basin (northern Italy). J. Quat. Sci. 35, 559–571.

662   https://doi.org/10.1002/jqs.3199

663   Burrato, P., Ciucci, F., Valensise, G., 2003. An inventory of river anomalies in the Po Plain, Northern

664   Italy: Evidence for active blind thrust faulting. Ann. Geophys. 46, 865–882.

665   https://doi.org/10.4401/ag-3459

666   Cacciari, M., Cremonini, S., Marchesini, M., Vianello, G., Antisari, L.V., 2017. When a pedomarker is

667   lacking: palynological and chemical multianalysis of a lateglacial-holocene soils suite

668   (Bologna). EQA-International J. Environ. Qual. 24, 47–73.

669   Cacciari, M., Amorosi, A., Marchesini, M., Kaniewski, D., Bruno, L., Campo, B., Rossi, V., 2020.

670   Linking Holocene vegetation dynamics , palaeoclimate variability and depositional patterns in

671   coastal successions : Insights from the Po Delta plain of northern Italy. Palaeogeogr.

672   Palaeoclimatol. Palaeoecol. 538, 109468. https://doi.org/10.1016/j.palaeo.2019.109468

673   Campo, B., Amorosi, A., Bruno, L., 2016. Contrasting alluvial architecture of Late Pleistocene and

674   Holocene deposits along a 120-km transect from the central Po Plain (northern Italy).

675   Sediment. Geol. 341, 265–275.

676   Campo, B., Bruno, L., Amorosi, A., 2020. Basin-scale stratigraphic correlation of late Pleistocene-

677   Holocene (MIS 5e-MIS 1) strata across the rapidly subsiding Po Basin (northern Italy). Quat.

678   Sci. Rev. 237, 106300. https://doi.org/10.1016/j.quascirev.2020.106300

679   Chappell, J., 2002. Sea level changes forced ice breakouts in the Last Glacial cycle: New results

680   from coral terraces. Quat. Sci. Rev. 21, 1229–1240. https://doi.org/10.1016/S0277-

681   3791(01)00141-X

682   Chen, S., Huang, Y., Zou, J., Shi, Y., 2013. Mean residence time of global topsoil organic carbon

683   depends on temperature, precipitation and soil nitrogen. Glob. Planet. Change 100, 99–108.

684   https://doi.org/10.1016/j.gloplacha.2012.10.006

685   Chichagova, O.A., Cherkinsky, A.E., 1993. Problems in radiocarbon dating of soils. Radiocarbon 35,

686   351–362. https://doi.org/10.1017/S0033822200060355

687   Choi, K., 2005. Pedogenesis of late Quaternary deposits, northern Kyonggi Bay, Korea: Implications

688   for relative sea-level change and regional stratigraphic correlation. Palaeogeogr.

689   Palaeoclimatol. Palaeoecol. 220, 387–404. https://doi.org/10.1016/j.palaeo.2005.02.006

690   Clark, P.U., Huybers, P., 2009. Global change: Interglacial and future sea level. Nature 462, 856–

691   857. https://doi.org/10.1038/462856a

692   Cleveland, D.M., Atchley, S.C., Nordt, L.C., 2007. Continental sequence stratigraphy of the Upper

693   Triassic (Norian-Rhaetian) chinle strata, northern New Mexico, U.S.A.: Allocyclic and

694   autocyclic origins of paleosol-bearing alluvial successions. J. Sediment. Res. 77, 909–924.

695   https://doi.org/10.2110/jsr.2007.082

696   Cohen, K.M., Gouw, M.J.P., Holten, J.P., 2003. Fluvio-deltaic floodbasin deposits recording

697   differential subsidence within a coastal prism (central Rhine-Meuse delta, the Netherlands).

698   Ned. Geogr. Stud. 40–68. https://doi.org/10.1002/9781444304350.ch17

699   Cremaschi, M., 1987. Paleosols and Vetusols in the Central Po Plain (Northern Italy): a study in

700   Quaternary geology and soil development, Unicopli. ed. Paleosols and Vetusols in the Central

701   Po Plain (Northern Italy): A Study in Quaternary Geology and Soil Development., Milano.

702   Cremaschi, M., Nicosia, C., 2012. Sub-Boreal aggradation along the Apennine margin of the Central

703   Po Plain: geomorphological and geoarchaeological aspects. Géomorphologie Reli. Process.

704   Environ. 18, 155–174.

705   Demko, T.M., Currie, B.S., Nicoll, K.A., 2004. Regional paleoclimatic and stratigraphic implications

706   of paleosols and fluvial/overbank architecture in the Morrison Formation (Upper Jurassic),

707   Western Interior, USA. Sediment. Geol. 167, 115–135.

708   https://doi.org/10.1016/j.sedgeo.2004.01.003

709   Diessel, C.F.K., 1992. Coal facies and depositional environment, in: Coal-Bearing Depositional

710   Systems. Springer, pp. 161–264.

711   Dubiel, R.F., Hasiotis, S.T., 2011. Deposystems, paleosols, and climatic variability in a continental

712   system: the Upper Triassic Chinle Formation, Colorado Plateau, USA. From River to Rock Rec.

713   Preserv. Fluv. Sediments their Subseq. Interpret. SEPM (Society Sediment. Geol. Spec. Publ.

714   97, 393–421.

715   Fantoni, R., Bersezio, R., Forcella, F., 2004. Alpine structure and deformation chronology at the

716   Southern Alps-Po Plain border in Lombardy. Boll. della Soc. Geol. Ital. 123, 463–476.

717 Feng, Y., 2009. Fundamental considerations of soil organic carbon dynamics: a new theoretical

718   framework. Soil Sci. 174, 467–481.

719 Fletcher, W.J., Sánchez Goñi, M.F., Allen, J.R.M., Cheddadi, R., Combourieu-Nebout, N., Huntley,

720   B., Lawson, I., Londeix, L., Magri, D., Margari, V., Müller, U.C., Naughton, F., Novenko, E.,

721   Roucoux, K., Tzedakis, P.C., 2010. Millennial-scale variability during the last glacial in

722   vegetation records from Europe. Quat. Sci. Rev. 29, 2839–2864.

723   https://doi.org/10.1016/j.quascirev.2009.11.015

724 Fontaine, S., Barot, S., Barré, P., Bdioui, N., Mary, B., Rumpel, C., 2007. Stability of organic carbon

725   in deep soil layers controlled by fresh carbon supply. Nature 450, 277–280.

726   https://doi.org/10.1038/nature06275

727 Fontana, A., Mozzi, P., Marchetti, M., 2014. Alluvial fans and megafans along the southern side of

728   the Alps. Sediment. Geol. 301, 150–171. https://doi.org/10.1016/j.sedgeo.2013.09.003

729 Garzanti, E., Vezzoli, G., Andò, S., 2011. Paleogeographic and paleodrainage changes during

730   Pleistocene glaciations (Po Plain, Northern Italy). Earth-Science Rev. 105, 25–48.

731   https://doi.org/10.1016/j.earscirev.2010.11.004

732 Gaudinski, J., Trumbore, S., Davidson, E., 2000. Soil carbon cycling in a temperate forest:

733   radiocarbon-based estimates of residence times, …. Biogeochemistry 51, 33–69.

734 Geyh, M.A., Roeschmann, G., Wijmstra, T.A., Middeldorp, A.A., 1983. The Unreliability of 14 C

735   Dates Obtained from Buried Sandy Podzols . Radiocarbon 25, 409–416.

736   https://doi.org/10.1017/s0033822200005695

737 Ghielmi, M., Minervini, M., Nini, C., Rogledi, S., Rossi, M., 2013. Late Miocene-Middle Pleistocene

738   sequences in the Po Plain - Northern Adriatic Sea (Italy): The stratigraphic record of

739   modification phases affecting a complex foreland basin. Mar. Pet. Geol. 42, 50–81.

740   https://doi.org/10.1016/j.marpetgeo.2012.11.007

741   Gibling, M.R., Bird, D.J., 1994. Late Carboniferous cyclothems and alluvial paleovalleys in the

742   Sydney Basin, Nova Scotia. Geol. Soc. Am. Bull. 106, 105–117. https://doi.org/10.1130/0016-

743   7606(1994)106<0105:LCCAAP>2.3.CO;2

744   Gibling, M.R., Fielding, C.R., Sinha, R., Davidson, S.K., Leleu, S., North, C.P., 2011. Alluvial valleys

745   and alluvial sequences: towards a geomorphic assessment. From River to Rock Rec. Preserv.

746   Fluv. Sediments Their Subseq. Interpret. SEPM, Spec. Publ. 97, 423–447.

747   Gile, L.H., Hawley, J.W., Grossman, R.B., 1981. Soils and geomorphology in the Basin and Range

748   area of southern New Mexico: Guidebook to the Desert Project, New Mexico, Bureau of

749   Mines and Mineral Resources Memoir.

750   Gilet-Blein, N., Marien, G., Evin, J., 1980. of and of of and. Radiocarbon 22, 919–929.

751   Gunderson, K.L., Pazzaglia, F.J., Picotti, V., Anastasio, D.A., Kodama, K.P., Rittenour, T., Frankel,

752   K.F., Ponza, A., Berti, C., Negri, A., Sabbatini, A., 2014. Unraveling tectonic and climatic

753   controls on synorogenic growth strata (Northern Apennines, Italy). Bull. Geol. Soc. Am. 126,

754   532–552. https://doi.org/10.1130/B30902.1

755   Hajek, E.A., Wolinsky, M.A., 2012. Simplified process modeling of river avulsion and alluvial

756   architecture: Connecting models and field data. Sediment. Geol. 257–260, 1–30.

757   https://doi.org/10.1016/j.sedgeo.2011.09.005

758   Helmens, K.F., 2014. The last interglacial-glacial cycle (MIS 5-2) re-examined based on long proxy

759   records from central and northern europe. Quat. Sci. Rev. 86, 115–143.

760   https://doi.org/10.1016/j.quascirev.2013.12.012

761   Hijma, M.P., Cohen, K.M., 2011. Holocene transgression of the Rhine river mouth area, The

762   Netherlands/Southern North Sea: Palaeogeography and sequence stratigraphy.

763   Sedimentology 58, 1453–1485. https://doi.org/10.1111/j.1365-3091.2010.01222.x

764   Hofmann, F., Reichenbacher, B., Farley, K.A., 2017. Evidence for >5 Ma paleo-exposure of an

765   Eocene–Miocene paleosol of the Bohnerz Formation, Switzerland. Earth Planet. Sci. Lett. 465,

766   168–175. https://doi.org/10.1016/j.epsl.2017.02.042

767   Holbrook, J., Schumm, S.A., 1999. Geomorphic and sedimentary response of rivers to tectonic

768   deformation: A brief review and critique of a tool for recognizing subtle epeirogenic

769   deformation in modern and ancient settings. Tectonophysics 305, 287–306.

770   https://doi.org/10.1016/S0040-1951(99)00011-6

771   Hošek, J., Lisá, L., Hambach, U., Petr, L., Vejrostová, L., Bajer, A., Grygar, T.M., Moska, P., Gottvald,

772   Z., Horsák, M., 2017. Middle Pleniglacial pedogenesis on the northwestern edge of the

773   Carpathian basin: A multidisciplinary investigation of the Bíňa pedo-sedimentary section, SW

774   Slovakia. Palaeogeogr. Palaeoclimatol. Palaeoecol. 487, 321–339.

775   https://doi.org/10.1016/j.palaeo.2017.09.017

776   Ishii, Y., Hori, K., Momohara, A., Nakanishi, T., Hong, W., 2016. Middle to late-Holocene decreased

777   fluvial aggradation and widespread peat initiation in the Ishikari lowland (northern Japan).

778   The Holocene 26, 1924–1938.

779   Janssens, M.M., Kasse, C., Bohncke, S.J.P., Greaves, H., Cohen, K.M., Wallinga, J., Hoek, W.Z., 2012.

780   Climate-driven fluvial development and valley abandonment at the last glacial-interglacial

781   transition (Oude IJssel-Rhine, Germany). Geol. en Mijnbouw/Netherlands J. Geosci. 91, 37–

782   62. https://doi.org/10.1017/s001677460000055x

783   Kaiser, K., Hilgers, A., Schlaak, N., Jankowski, M., Kühn, P., Bussemer, S., Przegietka, K., 2009.

784   Palaeopedological marker horizons in northern central Europe: Characteristics of Lateglacial

785   Usselo and Finow soils. Boreas 38, 591–609. https://doi.org/10.1111/j.1502-

786   3885.2008.00076.x

787   Kalisz, B., Lachacz, A., Glazewski, R., 2010. Transformation of some organic matter components in

788   organic soils exposed to drainage. Turkish J. Agric. For. 34, 245–256.

789   https://doi.org/10.3906/tar-0905-33

790   Kleber, M., 2010. What is recalcitrant soil organic matter? Environ. Chem. 7, 320–332.

791   https://doi.org/10.1071/EN10006

792   Kosters, E.C., Suter, J.R., 1993. Facies relationships and systems tracts in the late Holocene

793   Mississippi Delta Plain. J. Sediment. Petrol. 63, 727–733. https://doi.org/10.1306/D4267BCC-

794   2B26-11D7-8648000102C1865D

795   Kraus, M.J., 1999. Paleosols in clastic sedimentary rocks: Their geologic applications. Earth Sci. Rev.

796   47, 41–70. https://doi.org/10.1016/S0012-8252(99)00026-4

797   Kraus, M.J., Bown, T.M., 1993. Palaeosols and sandbody prediction in alluvial sequences. Geol.

798   Soc. London, Spec. Publ. 73, 23–31.

799   Kvale, E.P., Archer, A.W., 2007. Paleovalley fills: Trunk vs. tributary. Am. Assoc. Pet. Geol. Bull. 91,

800   809–821. https://doi.org/10.1306/11060606022

801   Lambeck, K., Antonioli, F., Anzidei, M., Ferranti, L., Leoni, G., Scicchitano, G., Silenzi, S., 2011. Sea

802   level change along the Italian coast during the Holocene and projections for the future. Quat.

803   Int. 232, 250–257. https://doi.org/10.1016/j.quaint.2010.04.026

804   Larionova, A.A., Maltseva, A.N., Lopes de Gerenyu, V.O., Kvitkina, A.K., Bykhovets, S.S., Zolotareva,

805   B.N., Kudeyarov, V.N., 2017. Effect of temperature and moisture on the mineralization and

806   humification of leaf litter in a model incubation experiment. Eurasian Soil Sci. 50, 422–431.

807   https://doi.org/10.1134/S1064229317020089

808   Lewis, S.G., Maddy, D., Scaife, R.G., 2001. The fluvial system response to abrupt climate change

809   during the last cold stage: The Upper Pleistocene River Thames fluvial succession at Ashton

810   Keynes, UK. Glob. Planet. Change 28, 341–359. https://doi.org/10.1016/S0921-

811   8181(00)00083-7

812   Machette, M.N., 1985. Calcific soils of the southwestern United States. Soils Quat. Geol.

813   Southwest. United States Geol. Soc. Am. Spec. Pap. 203, 1–21.

814   Maestrelli, D., Benvenuti, M., Bonini, M., Carnicelli, S., Piccardi, L., Sani, F., 2018. The structural

815   hinge of a chain-foreland basin: Quaternary activity of the Pede-Apennine Thrust front

816   (Northern Italy). Tectonophysics 723, 117–135. https://doi.org/10.1016/j.tecto.2017.12.006

817   Magri, D., 1999. Late Quaternary vegetation history at Lagaccione near Lago di Bolsena (central

818   Italy). Rev. Palaeobot. Palynol. 106, 171–208. https://doi.org/10.1016/S0034-6667(99)00006-

819   8

820   Marabini, S., Vai G.B., 2020. Carta Geologica della Pianura tra Imola e Ravenna, Thèodolite Editore,

821   Imola, 81pp. (in Italian).

822   Martin, C.W., Johnson, W.C., 1995. Variation in radiocarbon ages of soil organic matter fractions

823   from late Quaternary buried soils. Quat. Res. 43, 232–237.

824   Matthews, J.A., 1980. Some Problems and Implications of 14C Dates from a Podzol Buried beneath

825   an End Moraine at Haugabreen , Southern Norway Author (s): John A . Matthews Published

826   by : Taylor & Francis , Ltd . on behalf of the Swedish Society for Anthropology and Geography

827   62, 185–208.

828   Matthews, J.A., 1981. Natural 14 C age/depth gradient in a buried soil. Naturwissenschaften 68,

829   472–474.

830   Matthews, J.A., Dresser, P.Q., 1983. Intensive 14C dating of a buried palaeosol horizon. Geol.

831   Föreningen i Stock. Förhandlingar 105, 59–63.

832   McCarthy, P.J., Plint, A.G., 1998. Recognition of interfluve sequence boundaries: integrating

833   paleopedology and sequence stratigraphy. Geology 26, 387–390.

834   https://doi.org/10.1130/0091-7613(1998)026<0387:ROISBI>2.3.CO;2

835   McCarthy, P.J., Plint, A.G., 2003. Spatial variability of palaeosols across Cretaceous interfluves in

836   the Dunvegan Formation, NE British Columbia, Canada: Palaeohydrological,

837   palaeogeomorphological and stratigraphic implications. Sedimentology 50, 1187–1220.

838   https://doi.org/10.1111/j.1365-3091.2003.00600.x

839   Meingast, K.M., Grunert, B.K., Green, S.A., Kane, E.S., Khademimoshgenani, N., 2020. Insights on

840   dissolved organic matter production revealed by removal of charge-transfer interactions in

841   senescent leaf leachates. Water (Switzerland) 12. https://doi.org/10.3390/W12092356

842   Miall, A.D., 1985. Architectural-element analysis: a new method of facies analysis applied to fluvial

843   deposits. Earth-Science Rev. 22, 261–308.

844   Moine, O., Antoine, P., Hatté, C., Landais, A., Mathieu, J., Prud'homme, C., Rousseau, D.D., 2017.

845   The impact of Last Glacial climate variability in west-European loess revealed by radiocarbon

846   dating of fossil earthworm granules. Proc. Natl. Acad. Sci. U. S. A. 114, 6209–6214.

847   https://doi.org/10.1073/pnas.1614751114

848   Mol, J., 1997. Fluvial response to Weichselian climate changes in the Niederlausitz (Germany). J.

849   Quat. Sci. 12, 43–60. https://doi.org/10.1002/(SICI)1099-1417(199701/02)12:1<43::AID-

850   JQS291>3.0.CO;2-0

851   Monegato, G., Scardia, G., Hajdas, I., Rizzini, F., Piccin, A., 2017. The Alpine LGM in the boreal ice-

852   sheets game. Sci. Rep. 7, 1–8. https://doi.org/10.1038/s41598-017-02148-7

853   Morelli, A., Bruno, L., Cleveland, D.M., Drexler, T.M., Amorosi, A., 2017. Reconstructing Last Glacial

854   Maximum and Younger Dryas paleolandscapes through subsurface paleosol stratigraphy: An

855   example from the Po coastal plain, Italy. Geomorphology 295, 790–800.

856   https://doi.org/10.1016/j.geomorph.2017.08.013

857   Mozzi, P., Bini, C., Zilocchi, L., Becattini, R., Lippi, M.M., 2003. Stratigraphy, palaeopedology and

858   palynology of late Pleistocene and Holocene deposits in the landward sector of the Lagoon of

859   Venice (Italy), in relation to the Caranto level. Alp. Mediterr. Quat. 16, 193–210.

860   Muttoni, G., Carcano, C., Garzanti, E., Ghielmi, M., Piccin, A., Pini, R., Rogledi, S., Sciunnach, D.,

861   2003. Onset of major Pleistocene glaciations in the Alps. Geology 31, 989–992.

862   https://doi.org/10.1130/G19445.1

863   Muttoni, G., Scardia, G., Kent, D. V., Morsiani, E., Tremolada, F., Cremaschi, M., Peretto, C., 2011.

864   First dated human occupation of Italy at ~0.85Ma during the late Early Pleistocene climate

865   transition. Earth Planet. Sci. Lett. 307, 241–252. https://doi.org/10.1016/j.epsl.2011.05.025

866   Orlova, L.A., Panychev, V.A., 1993. The reliability of radiocarbon dating buried soils. Radiocarbon

867   35, 369–377. https://doi.org/10.1017/S0033822200060379

868   Pandey, D., Agrawal, M., Singh Bohra, J., Adhya, T.K., Bhattacharyya, P., 2014. Recalcitrant and

869   labile carbon pools in a sub-humid tropical soil under different tillage combinations: A case

870   study of rice-wheat system. Soil Tillage Res. 143, 116–122.

871   https://doi.org/10.1016/j.still.2014.06.001

872   Pati, P., Verma, A.K., Dash, C., Patel, N.K., Gupta, A., Sharma, V., Jakhmola, R.P., Parkash, B.,

873   Awasthi, A.K., Saraf, A.K., 2019. Influence of neotectonism on geomorphology and

874   depositional architecture of the Gandak megafan, middle Ganga plain, India. Geomorphology

875   327, 489–503. https://doi.org/10.1016/j.geomorph.2018.11.029

876   Pellegrini, C., Asioli, A., Bohacs, K.M., Drexler, T.M., Feldman, H.R., Sweet, M.L., Maselli, V., Rovere,

877   M., Gamberi, F., Valle, G.D., Trincardi, F., 2018. The late Pleistocene Po River lowstand wedge

878   in the Adriatic Sea: Controls on architecture variability and sediment partitioning. Mar. Pet.

879   Geol. 96, 16–50. https://doi.org/10.1016/j.marpetgeo.2018.03.002

880   Peltier, W.R., Fairbanks, R.G., 2006. Global glacial ice volume and Last Glacial Maximum duration

881   from an extended Barbados sea level record. Quat. Sci. Rev. 25, 3322–3337.

882   https://doi.org/10.1016/j.quascirev.2006.04.010

883   Phillips, J.D., 2011. Universal and local controls of avulsions in southeast Texas Rivers.

884   Geomorphology 130, 17–28. https://doi.org/10.1016/j.geomorph.2010.10.001

885 Picotti, V., Pazzaglia, F.J., 2008. A new active tectonic model for the construction of the Northern

886   Apennines mountain front near Bologna (Italy). J. Geophys. Res. Solid Earth 113, 1–24.

887   https://doi.org/10.1029/2007JB005307

888 Pini, R., Ravazzi, C., Reimer, P.J., 2010. The vegetation and climate history of the last glacial cycle in

889   a new pollen record from Lake Fimon (southern Alpine foreland, N-Italy). Quat. Sci. Rev. 29,

890   3115–3137. https://doi.org/10.1016/j.quascirev.2010.06.040

891 Piovan, S., Mozzi, P., Zecchin, M., 2012. The interplay between adjacent Adige and Po alluvial

892   systems and deltas in the late Holocene (Northern Italy). Géomorphologie Reli. Process.

893   Environ. 18, 427–440.

894 Plint, A.G., Moore, J., Plint, A., Sanders, J., Ulic, D., 2001. stratigraphy : Updip expression Formation

895   , Alberta foreland. October 11, 1967–2001.

896 Rasbury, E.T., Hanson, G.N., Meyers, W.J., Saller, A.H., 1997. Dating of the time of sedimentation

897   using U-Pb ages for paleosol calcite. Geochim. Cosmochim. Acta 61, 1525–1529.

898   https://doi.org/10.1016/S0016-7037(97)00043-4

899 Rasmussen, S.O., Bigler, M., Blockley, S.P., Blunier, T., Buchardt, S.L., Clausen, H.B., Cvijanovic, I.,

900   Dahl-Jensen, D., Johnsen, S.J., Fischer, H., Gkinis, V., Guillevic, M., Hoek, W.Z., Lowe, J.J.,

901   Pedro, J.B., Popp, T., Seierstad, I.K., Steffensen, J.P., Svensson, A.M., Vallelonga, P., Vinther,

902   B.M., Walker, M.J.C., Wheatley, J.J., Winstrup, M., 2014. A stratigraphic framework for abrupt

903   climatic changes during the Last Glacial period based on three synchronized Greenland ice-

904   core records: Refining and extending the INTIMATE event stratigraphy. Quat. Sci. Rev. 106,

905   14–28. https://doi.org/10.1016/j.quascirev.2014.09.007

906 Ravazzi, C., Donegana, M., Vescovi, E., Arpenti, E., Caccianiga, M., Kaltenrieder, P., Londeix, L.,

907   Marabini, S., Mariani, S., Pini, R., Vai, G.B., Wick, L., 2006. A new Late-glacial site with Picea

908   abies in the northern Apennine foothills: An exception to the model of glacial refugia of trees.

909   Veg. Hist. Archaeobot. 15, 357–371. https://doi.org/10.1007/s00334-006-0055-9

910   Ravazzi, C., Deaddis, M., De Amicis, M., Marchetti, M., Vezzoli, G., Zanchi, A., 2012. Évolution de la

911   plaine centrale du Pô entre les rivières Adda et Serio au cours des 40 derniers millénaires.

912   Geomorphol. Reli. Process. Environ. 131–154. https://doi.org/10.4000/geomorphologie.9794

913   Regione Emilia-Romagna & Eni-Agip, 1998. Riserve idriche sotterranee della Regione Emilia-

914   Romagna. S.EL.CA, Firenze *(in Italian)*.

915   Reimer, P.J., Austin, W.E.N., Bard, E., Bayliss, A., Blackwell, P.G., Bronk Ramsey, C., Butzin, M.,

916   Cheng, H., Edwards, R.L., Friedrich, M., Grootes, P.M., Guilderson, T.P., Hajdas, I., Heaton, T.J.,

917   Hogg, A.G., Hughen, K.A., Kromer, B., Manning, S.W., Muscheler, R., Palmer, J.G., Pearson, C.,

918   Van Der Plicht, J., Reimer, R.W., Richards, D.A., Scott, E.M., Southon, J.R., Turney, C.S.M.,

919   Wacker, L., Adolphi, F., Büntgen, U., Capano, M., Fahrni, S.M., Fogtmann-Schulz, A., Friedrich,

920   R., Köhler, P., Kudsk, S., Miyake, F., Olsen, J., Reinig, F., Sakamoto, M., Sookdeo, A., Talamo,

921   S., 2020. The IntCal20 Northern Hemisphere Radiocarbon Age Calibration Curve (0-55 cal

922   kBP). Radiocarbon 62, 725–757. https://doi.org/10.1017/RDC.2020.41

923   Richardson, J.L., Vepraskas, M.J., 2001. Wetland soilsgenesis, hydrology, landscapes, and

924   classification.

925   Rousseau, D.D., Sima, A., Antoine, P., Hatté, C., Lang, A., Zöller, L., 2007. Link between European

926   and North Atlantic abrupt climate changes over the last glaciation. Geophys. Res. Lett. 34, 2–

927   7. https://doi.org/10.1029/2007GL031716

928   Rousseau, D.D., Antoine, P., Gerasimenko, N., Sima, A., Fuchs, M., Hatté, C., Moine, O., Zoeller, L.,

929   2011. North Atlantic abrupt climatic events of the last glacial period recorded in Ukrainian

930   loess deposits. Clim. Past 7, 221–234. https://doi.org/10.5194/cp-7-221-2011

931   Scharpenseel, H.W., 1971. Radiocarbon dating of soils--problems, troubles, hopes. Paleopedol.

932   Orig. Nat. Dating Paleosols. Pap. 77–88.

933   Shanley, K.W., McCabe, P.J., 1994. Perspectives on the sequence stratigraphy of continental strata.

934   Am. Assoc. Pet. Geol. Bull. 78, 544–568. https://doi.org/10.1306/bdff9258-1718-11d7-

935   8645000102c1865d

936   Synal, H.A., Stocker, M., and Suter, M., 2007. MICADAS: A new compact radiocarbon AMS system.

937   Nuclear Instruments & Methods in Physics Research Section B-Beam Interactions with

938   Materials and Atoms 259, 7-13. https://doi.org/10.1016/j.nimb.2007.01.138

939   Soares, M.V.T., Basilici, G., Lorenzoni, P., Colombera, L., Mountney, N.P., Martinelli, A.G., Ferreira

940   Mesquita, Á., da Silva Marinho, T., Vásconez García, R.G., Marconato, A., 2020. Landscape

941   and depositional controls on palaeosols of a distributive fluvial system (Upper Cretaceous,

942   Brazil). Sediment. Geol. 410, 105774. https://doi.org/10.1016/j.sedgeo.2020.105774

943   Soldati, M., Borgatti, L., Cavallin, A., De Amicis, M., Frigerio, S., Giardino, M., Mortara, G.,

944   Pellegrini, G.B., Ravazzi, C., Surian, N., Tellini, C., Zanchi, A., Alberto, W., Albanese, D., Chelli,

945   A., Corsini, A., Marchetti, M., Palomba, M., Panizza, M., 2006. Geomorphological evolution of

946   slopes and climate changes in Northern Italy during the late quaternary: Spatial and temporal

947   distribution of landslides and landscape sensitivity implications. Geogr. Fis. e Din. Quat. 29,

948   164–183.

949   Stolt, M.H., Rabenhorst, M.C., 2011. Introduction and historical development of subaqueous soil

950   concepts. 36: 1-14.

951   Storms, J.E.A., Weltje, G.J., Terra, G.J., Cattaneo, A., Trincardi, F., 2008. Coastal dynamics under

952   conditions of rapid sea-level rise: Late Pleistocene to Early Holocene evolution of barrier-

953   lagoon systems on the northern Adriatic shelf (Italy). Quat. Sci. Rev. 27, 1107–1123.

954   https://doi.org/10.1016/j.quascirev.2008.02.009

955   Stouthamer, E., Cohen, K.M., Gouw, M.J.P., 2011. Avulsion and its implications for fluvial-deltaic

956   architecture: insights from the Holocene Rhine-Meuse delta. SEPM Spec. Publ. 97, 215–232.

957   Synal HA, Stocker M, and Suter M. 2007. MICADAS: A new compact radiocarbon AMS system.

958   *Nuclear Instruments & Methods in Physics Research Section B-Beam Interactions with*

959   *Materials and Atoms* 259: 7-13.

960   Tebbens, L.A., Veldkamp, A., Westerhoff, W., Kroonenberg, S.B., 1999. Fluvial incision and channel

961   downcutting as a response to Late-glacial and Early Holocene climate change: The lower

962   reach of the river Meuse (Maas), The Netherlands. J. Quat. Sci. 14, 59–75.

963   https://doi.org/10.1002/(SICI)1099-1417(199902)14:1<59::AID-JQS408>3.0.CO;2-Z

964   Toonen, W.H.J., Kleinhans, M.G., Cohen, K.M., 2012. Sedimentary architecture of abandoned

965   channel fills. Earth Surf. Process. Landforms 37, 459–472. https://doi.org/10.1002/esp.3189

966   Törnqvist, T.E., 1993. HOLOCENE ALTERNATION OF MEANDERING AND ANASTOMOSING

967   Formation Kreftenheye Formation m below Dutch Ordnance Datum (O . D .) _ Twent ~ e F ~

968   rmation ~ Betuwe and Formation Broek Formation / T ~ wente Formation. J. Sediment.

969   Petrol. 63, 683–693.

970   Trendell, A.M., Atchley, S.C., Nordt, L.C., 2012. Depositional and diagenetic controls on reservoir

971   attributes within a fluvial outcrop analog: Upper Triassic Sonsela member of the Chinle

972   Formation, Petrified Forest National Park, Arizona. Am. Assoc. Pet. Geol. Bull. 96, 679–707.

973   https://doi.org/10.1306/08101111025

974   Tsatskin, A., Sandler, A., Avnaim-Katav, S., 2015. Quaternary subsurface paleosols in Haifa Bay,

975   Israel: A new perspective on stratigraphic correlations in coastal settings. Palaeogeogr.

976   Palaeoclimatol. Palaeoecol. 426, 285–296. https://doi.org/10.1016/j.palaeo.2015.03.018

977   van Balen, R.T., Busschers, F.S., Tucker, G.E., 2010. Modeling the response of the Rhine-Meuse

978   fluvial system to Late Pleistocene climate change. Geomorphology 114, 440–452.

979   https://doi.org/10.1016/j.geomorph.2009.08.007

980   Vandenberghe, J., 2003. Climate forcing of fluvial system development: An evolution of ideas.

981   Quat. Sci. Rev. 22, 2053–2060. https://doi.org/10.1016/S0277-3791(03)00213-0

982   Vannoli, P., Burrato, P., Valensise, G., 2015. The Seismotectonics of the Po Plain (Northern Italy):

983   Tectonic Diversity in a Blind Faulting Domain. Pure Appl. Geophys. 172, 1105–1142.

984   https://doi.org/10.1007/s00024-014-0873-0

985   Vescovi, E., Ammann, B., Ravazzi, C., Tinner, W., 2010. A new Late-glacial and Holocene record of

986   vegetation and fire history from Lago del Greppo, northern Apennines, Italy. Veg. Hist.

987   Archaeobot. 19, 219–233. https://doi.org/10.1007/s00334-010-0243-5

988   Viseras, C., Calvache, M.L., Soria, J.M., Fernńdez, J., 2003. Differential features of alluvial fans

989   controlled by tectonics or eustatic accommodation space. Examples from the Betic Cordillera,

990   Spain. Geomorphology 50, 181–202. https://doi.org/10.1016/S0169-555X(02)00214-3

991   Wadsworth, J., Boyd, R., Diessel, C., Leckie, D., 2003. Stratigraphic style of coal and non-marine

992   strata in a high accommodation setting: Falher Member and Gates Formation (Lower

993   Cretaceous), western Canada. Bull. Can. Pet. Geol. 51, 275–303.

994   https://doi.org/10.2113/51.3.275

995   Wright, V.P., Marriott, S.B., 1993. The sequence stratigraphy of fluvial depositional systems: the

996   role of floodplain sediment storage. Sediment. Geol. 86, 203–210.

997   Zeeden, C., Hambach, U., Veres, D., Fitzsimmons, K., Obreht, I., Bösken, J., Lehmkuhl, F., 2018.

998   Millennial scale climate oscillations recorded in the Lower Danube loess over the last glacial

999   period. Palaeogeogr. Palaeoclimatol. Palaeoecol. 509, 164–181.

1000   https://doi.org/10.1016/j.palaeo.2016.12.029

1001   Zerboni, A., Trombino, L., Frigerio, C., Livio, F., Berlusconi, A., Michetti, A.M., Rodnight, H., Spötl,

1002   C., 2015. The loess-paleosol sequence at Monte Netto: a record of climate change in the

1003   Upper Pleistocene of the central Po Plain, northern Italy. J. Soils Sediments 15, 1329–1350.
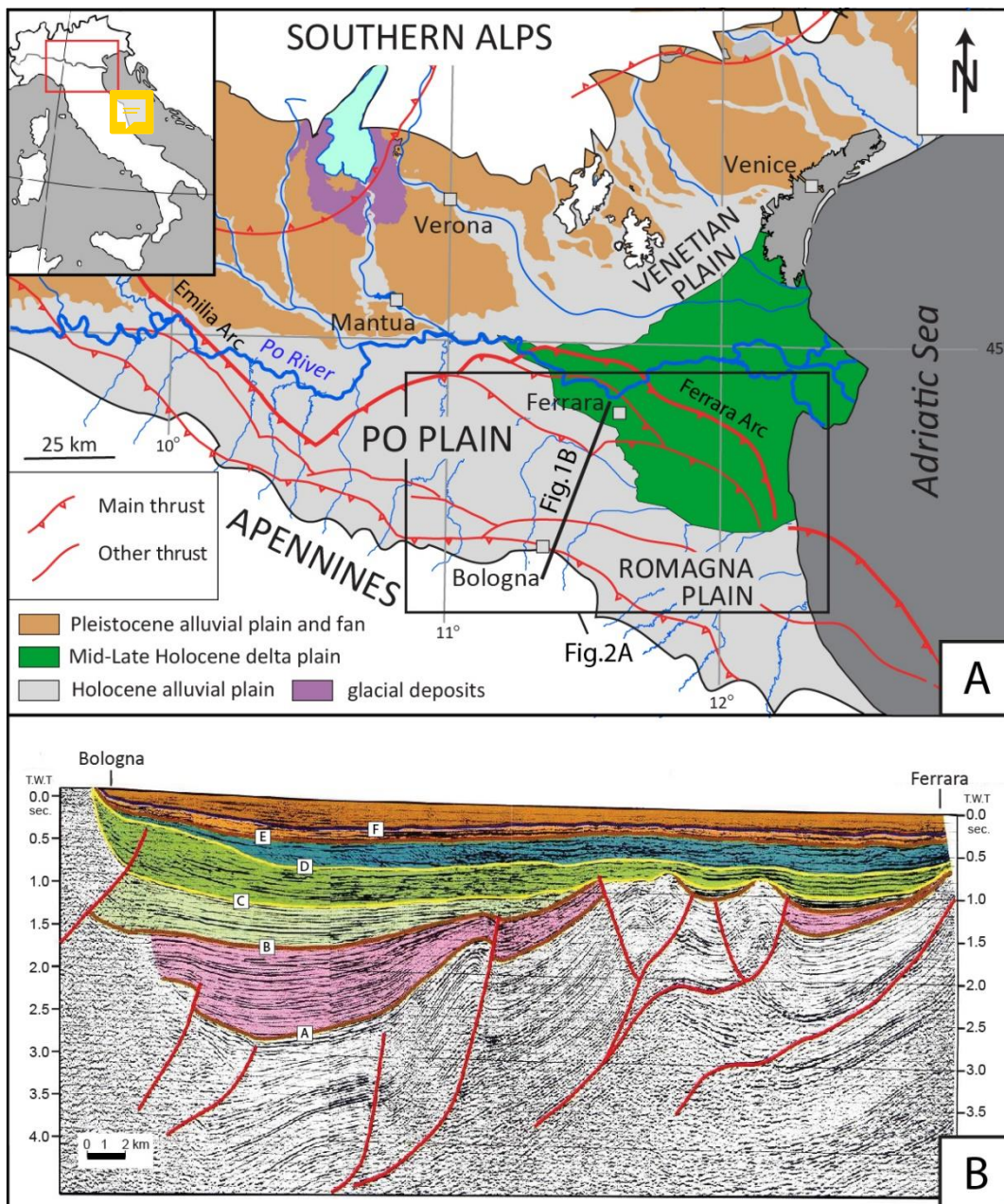
1004   https://doi.org/10.1007/s11368-014-0932-2

1005 Zuffetti, C., Trombino, L., Zembo, I., Bersezio, R., 2018. Soil evolution and origin of landscape in a

1006   late Quaternary tectonically mobile setting: The Po Plain-Northern Apennines border in

1007   Lombardy (Italy). Catena 171, 376–397. https://doi.org/10.1016/j.catena.2018.07.026

1008

1009

Figures and captions

1011

1012

1013 Fig. 1 – A. Geological map of the Po Plain, with location of the study area and of the seismic profile

1014 of Fig. 1B (modified after Bruno et al., 2019). The extent of Pleistocene alluvial deposits is from

1015 Fontana et al. (2014). Buried structures are modified after Burrato et al., (2003). B. Interpreted deep

1016 seismic profile (from Regione Emilia-Romagna & Eni-Agip, 1998, location in Figure 1A), with

1017 identification of the major blind thrusts (red lines) and main stratigraphic unconformities (lines from

1018 A–F) within the Po Basin fill (coloured area).

1019
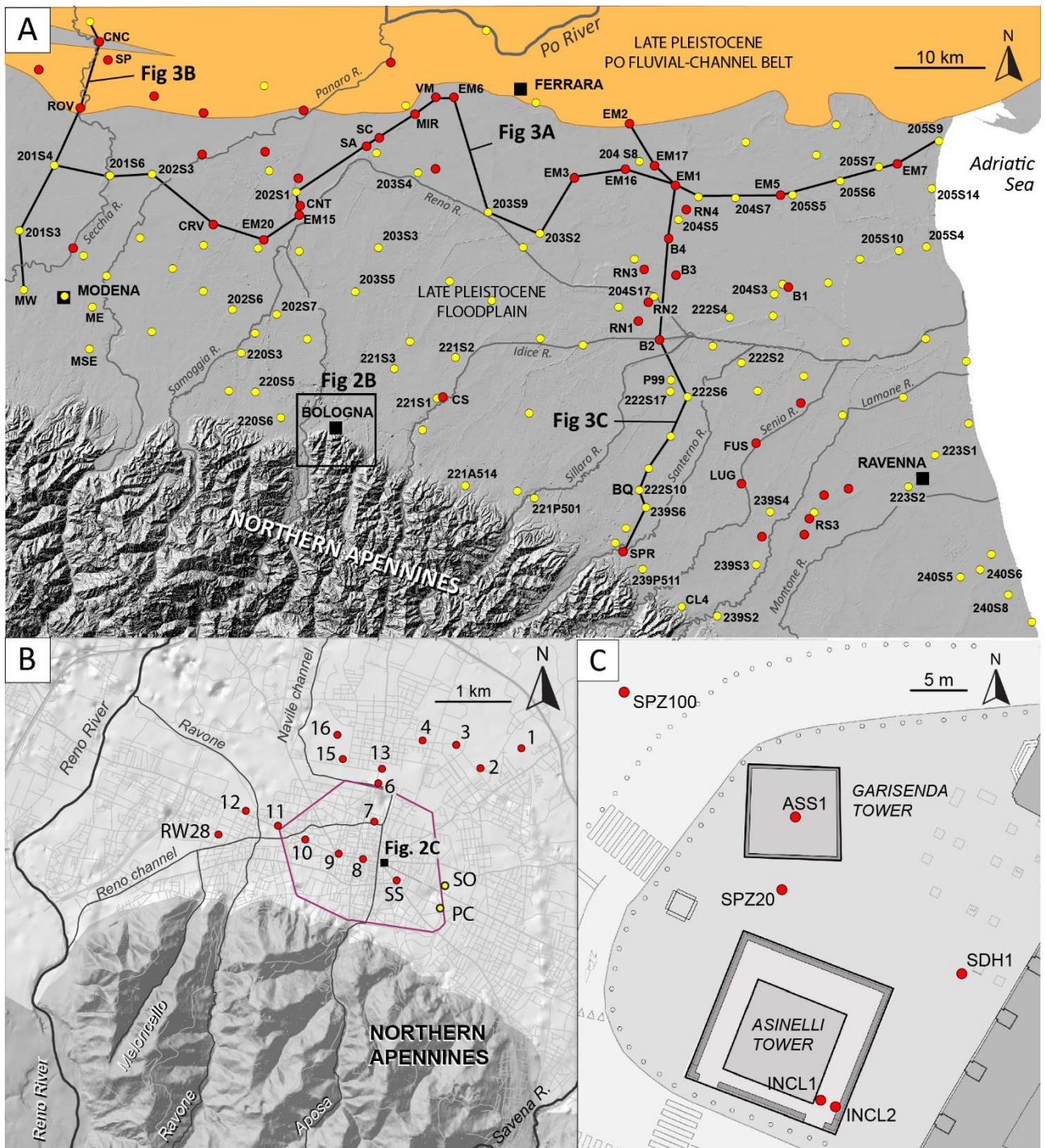
1020

1021 Fig. 2 – A. Study area with location of cores (red circles), core descriptions (yellow circles) and cross-

1022 sections of Fig. 5. B. Close-up on the Bologna area, with location of cores shown in Fig. 6. C. Location

1023 of cores drilled in the Two-Towers Medieval district (modified after Bruno et al., 2020b).

1024
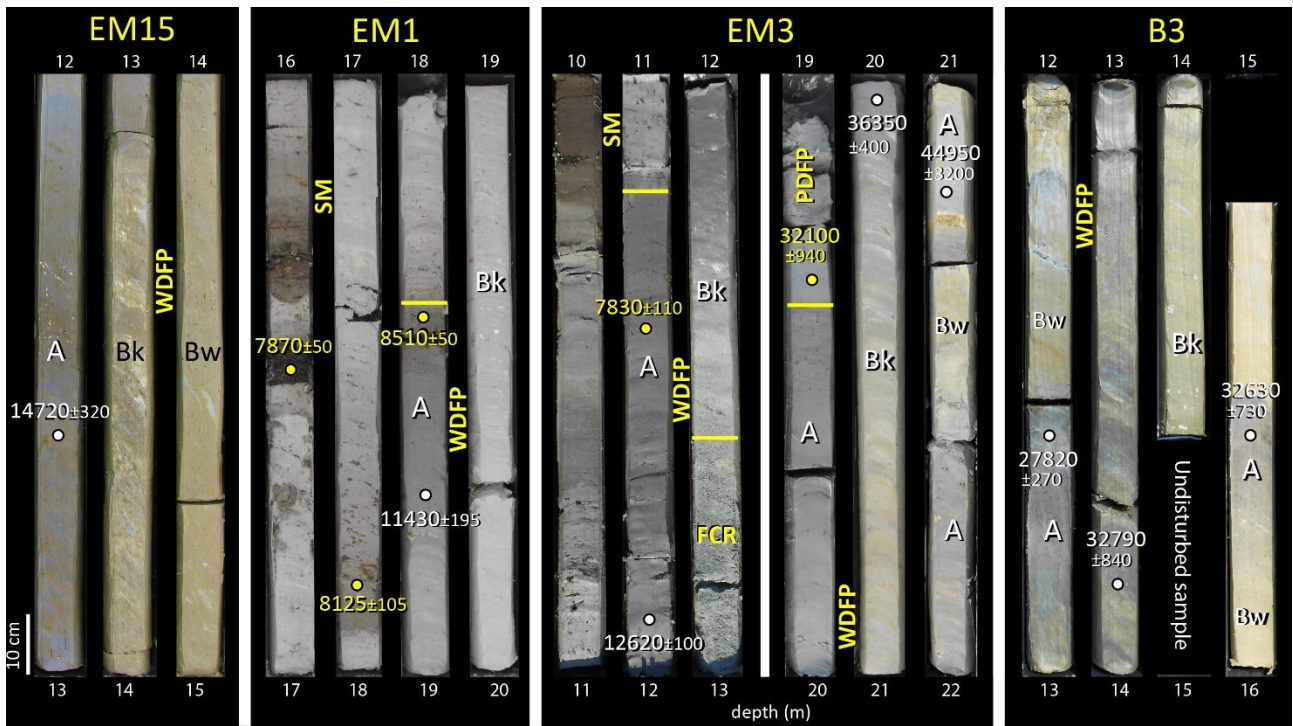
Fig. 3 – Representative photographs of paleosols from cores EM1, EM3 and B3 (location in Fig. 2).
WDFP: well-drained floodplain; PDFP: poorly-drained floodplain; SW: swamp; FCR: fluvial-channel-
related deposits. For pedological horizons A, Bk and Bw, see text. The white dates (cal kyr B.P.) are
from bulk-sediment samples, whereas the yellow ones are from plant macrofossils.

1031

Fig. 4 – Sedimentological characters and radiocarbon ages of paleosols P2, P3, PH and H1 from cores

RW28, 16, 17, EM1, EM20 and B3 (for location see Fig. 2). DOM: dissolved organic matter; UOM:

undecomposed organic matter; RF: redoximorphic features; CC carbonate concretions (the number

indicates the evolutionary stage, from Gile et al., 1981; Machette et al., 1985). WDFP: well-drained

floodplain; PDFP: poorly-drained floodplain; SW: swamp; FCR: fluvial-channel-related deposits. The black dates (cal kyr B.P.) are from bulk-sediment samples, whereas the red ones are from plant macrofossils.
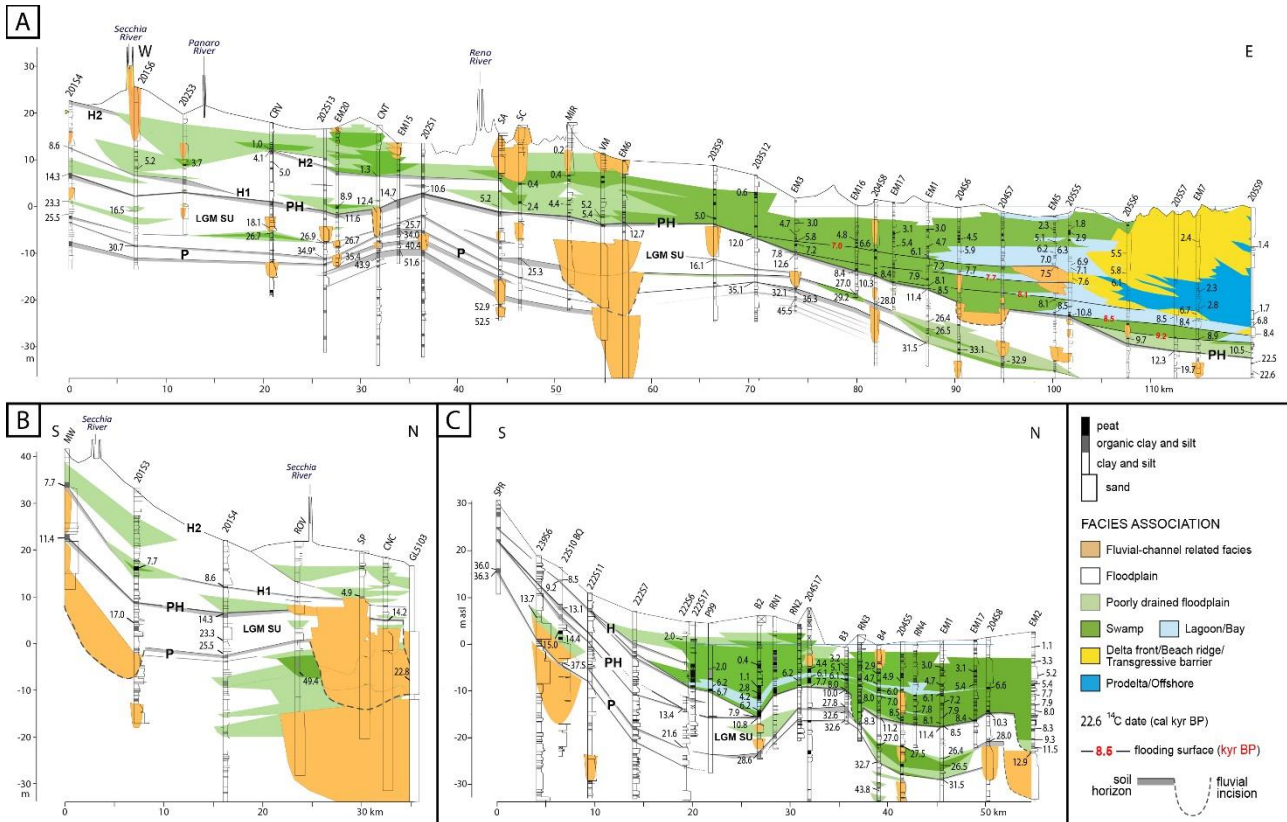
Fig. 5 – Upper Pleistocene and Holocene stratigraphy of the Po Plain depicted in cross-sections with W-E (A) and S-N (B and C) orientations (location in Fig. 2A). LGM SU: Last Glacial Maximum Stratigraphic Unit.

1046
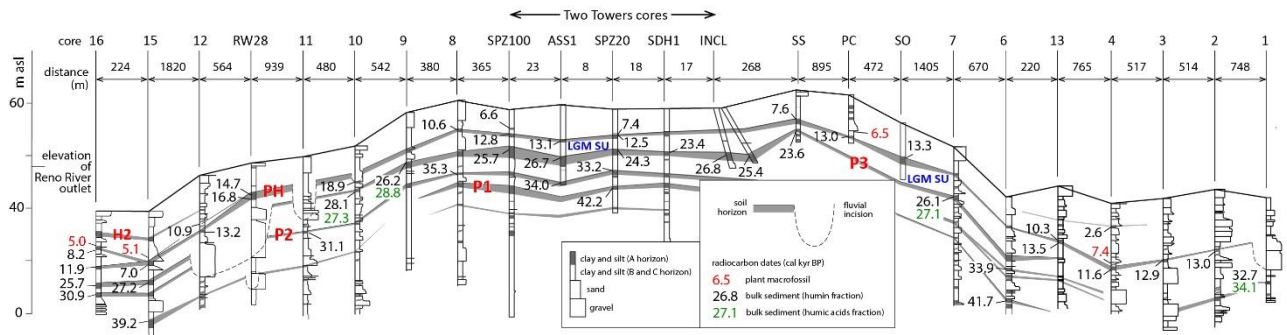
Fig. 6 – Paleosol-based correlations in the Bologna Area. LGM SU: Last Glacial Maximum

Stratigraphic Unit. Location of cores in Fig 2.

1047

1048

1049

1050

1051
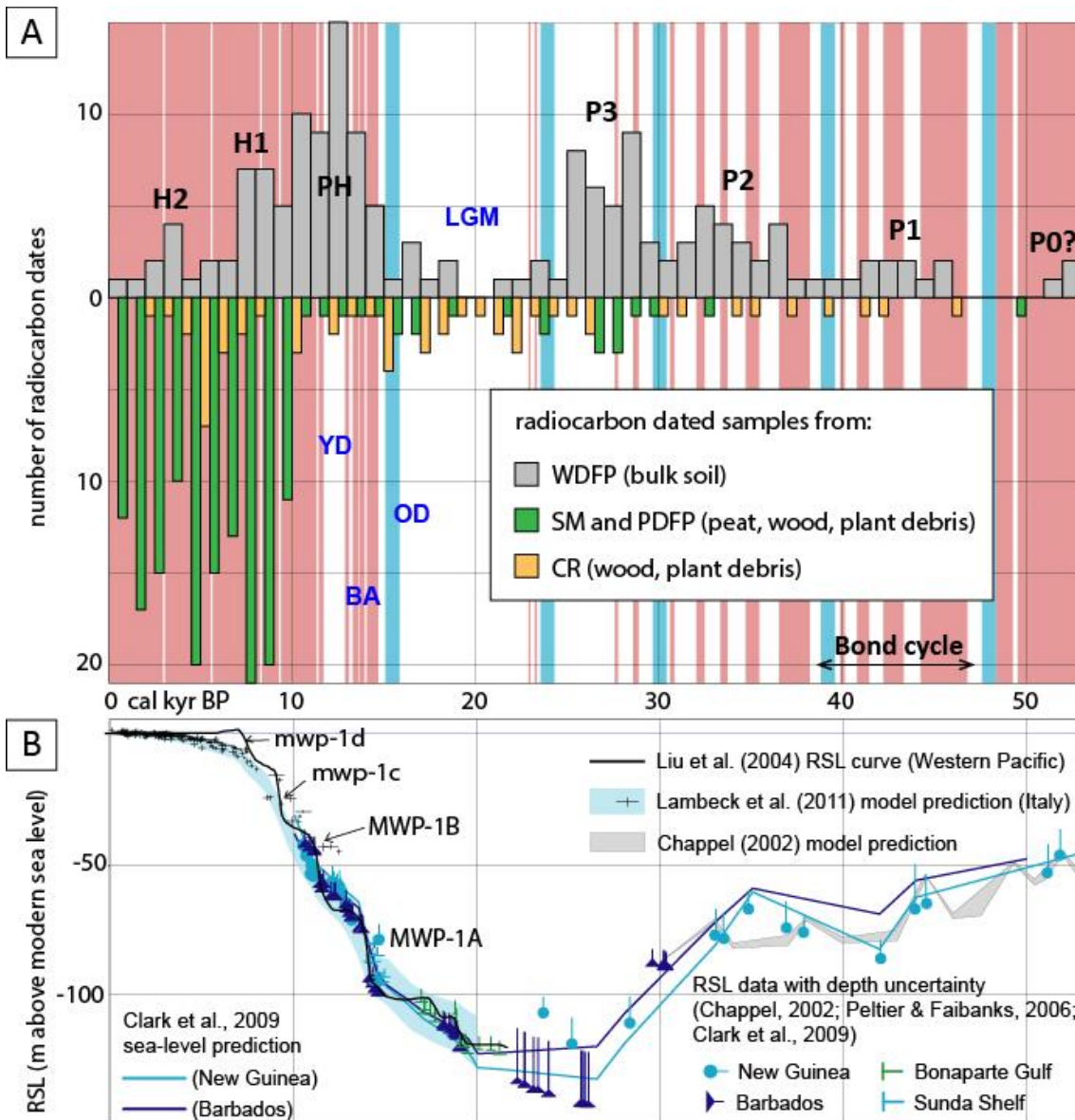
1052

Fig. 7 – A. Distribution of radiocarbon dates from bulk-soil and plant-macrofossil samples. A major

peak in dates from bulk-soil samples corresponds to paleosol PH; five minor peaks are related to

paleosols P1, P2, P3, H1 and H2. Notable is the lack of radiocarbon dated soils around 20 cal ky B.P.

(LGM). The sharp increase in radiocarbon dates from plant-macrofossils after 10 ky B.P., paralleled

by a decline in the number of dates from bulk-soil samples, reflects the onset of estuarine-deltaic

sedimentation in the distal Po Plain and the burial of paleosol PH. Red areas correspond to

interstadials, according to Bond et al., (1997) and Rasmussen et al. (2014). OD: Oldest Dryas; YD:

Younger Dryas. Light blue vertical bars indicate Henrich events (Bond et al., 1992). B. Sea-level

oscillations during the last 50 ky.
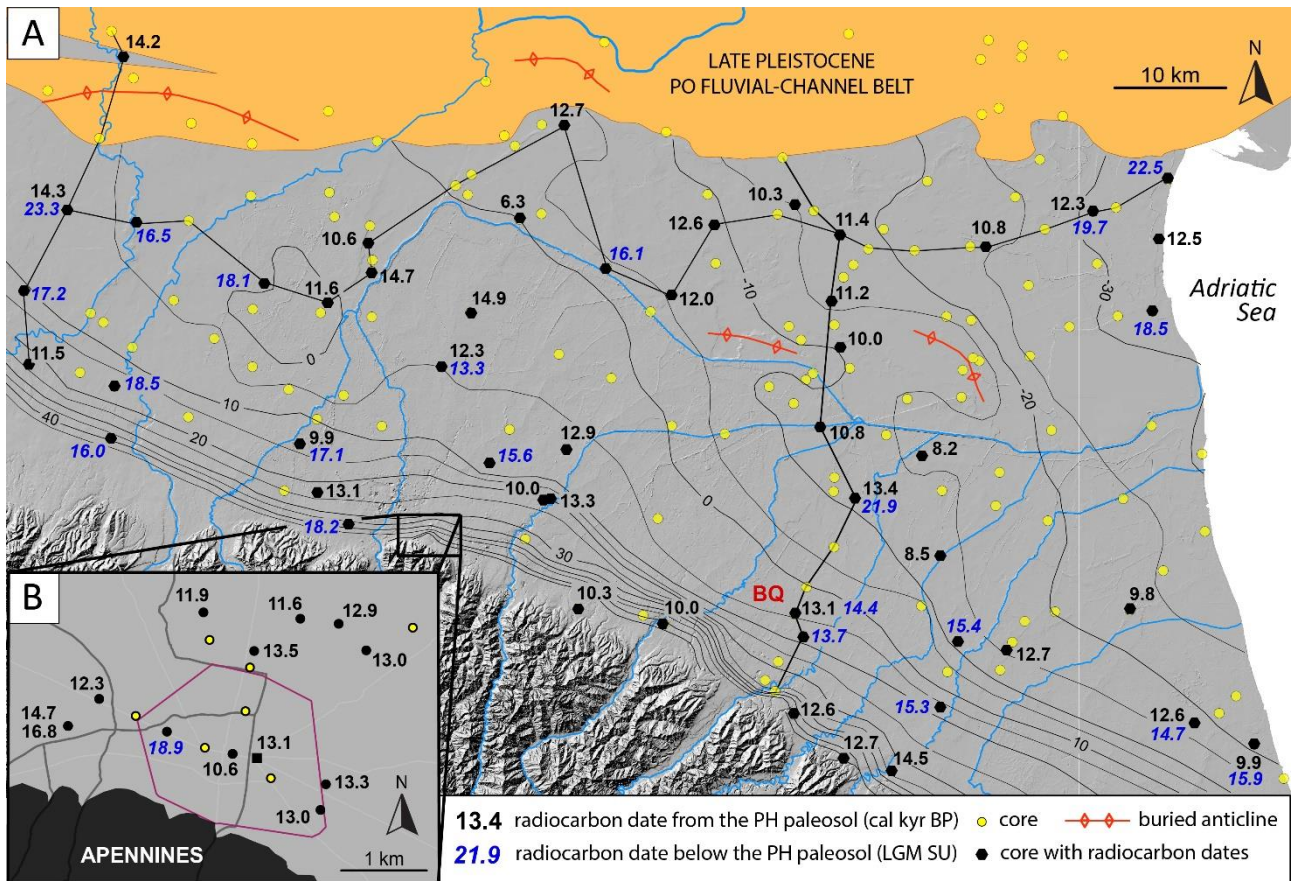
1062

Fig. 8 – Radiocarbon dates (black numbers, cal ky B.P.) from paleosol PH (bulk soil samples) in the Po Plain (A) and in the Bologna urban area (B). Blue numbers are the youngest ages from the underlying LGM stratigraphic unit. The present-day elevation (metres above modern sea-level) of paleosol PH is depicted through 5 m-spaced isolines. BQ: Bubano Quarry.
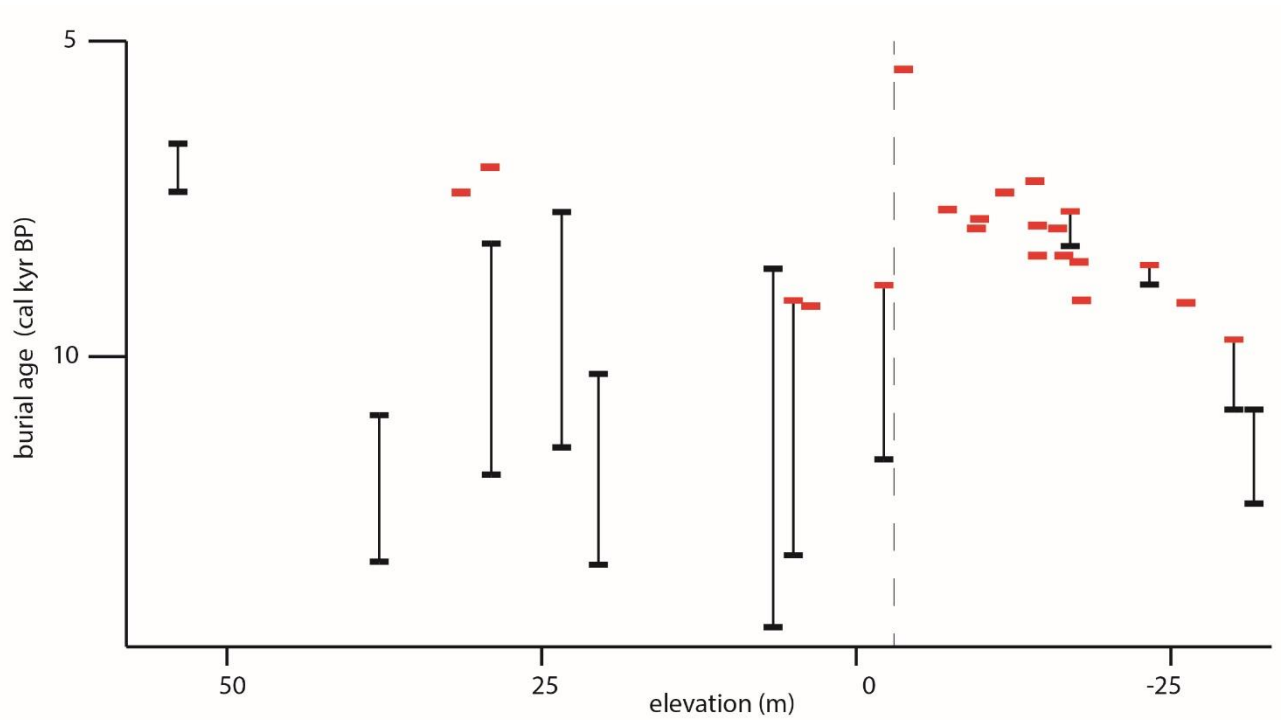
1068

1069   Fig. 9 – Burial ages of paleosol PH plotted against its present-day elevation (metres above modern

1070   sea-level). Black rectangles are radiocarbon dates from bulk soil samples. Red rectangles are

1071   radiocarbon dates from plant macrofossils. Burial ages from samples at elevation < - 3 m (dashed

1072   line) show an overall inverse proportionality with elevation. On the contrary, no specific trends are

1073   observable in burial-age distribution at elevation > - 3 m.

1074
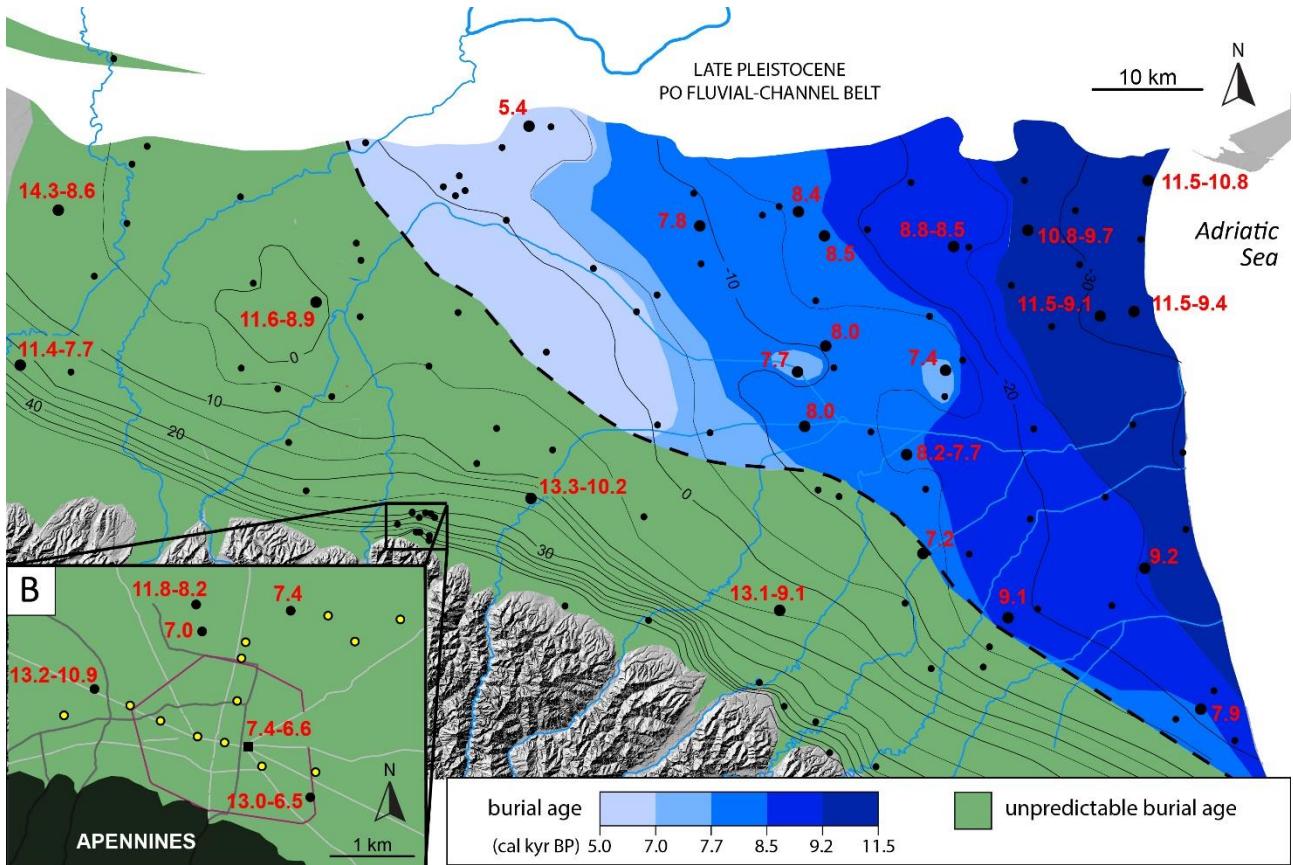
1075

Fig. 10 – Map showing burial ages (cal kyr B.P.) of paleosol PH in the Po Plain (A) and in the Bologna

urban area (B). The shades of blue depict progressively younger burial ages upland. In the green

area burial ages do not show specific spatial trends. Red numbers represent burial ages or intervals

measured along single cores (black circles). The map also depicts the present-day elevation (metres

above modern sea-level) of paleosol PH through 5 m-spaces isolines. Black dots are the countered

data points. The dashed line represents the maximum landward extent of Holocene estuarine and

delta plain deposits.

Figure 1

Click here to access/download;Figure;Fig. 1.jpg

Figure 2

Figure 3 Click here to access/download;Figure;Fig. 3.jpg ±

RW28

depth (m)		lithology	colour	consistency	accessory material	reaction to HCl	facies association
6 14720±720	PH	clayey silt	brown (10 YR 4/4)	hard	DOM, RF	weak	WDFP (A horizon)
16760±100			wheat (10 YR 8/4)		CC (3), RF	strong	WDFP (Bk horizon)

13

depth (m)		lithology	colour	consistency	accessory material	reaction to HCl	facies association
10 10340±120	PH	clayey silt	brown (10 YR 3/3)	hard	DOM, RF	weak	WDFP (A horizon)
11880±120			beige (10 YR 8/2)		CC (1, 2)	strong	WDFP (Bk horizon)
13540±80							

16

depth (m)		lithology	colour	consistency	accessory material	reaction to HCl	facies association
5050±210	H1	silty clay	brown (7.5YR 5/1)	firm	DOM, RF, Eneolithic artifacts	weak	WDFP (A horizon)
8210±160		clayey silt	grey (7.5YR 6/1) with orange mottles		RF		WDFP (Bw horizon)
		clayey and sandy silt				moderate	FCR
		silty clay with silt intercaltaions	grey (7.5YR 6/1)	weak			PDFP
11870±270	PH		dark grey (10YR 3/1)		DOM, UOM on top	weak	WDFP (A horizon)
			grey (5Y 7/1)	firm	CC (2), RF	strong	WDFP (Bk horizon)
		clayey silt					
25850±660	P3		dark grey (5Y 4/1)	hard	DOM, RF	weak	WDFP (A horizon)
			olive grey (5Y 6/1)		CC (2), RF	strong	WDFP (Bk horizon)

EM20

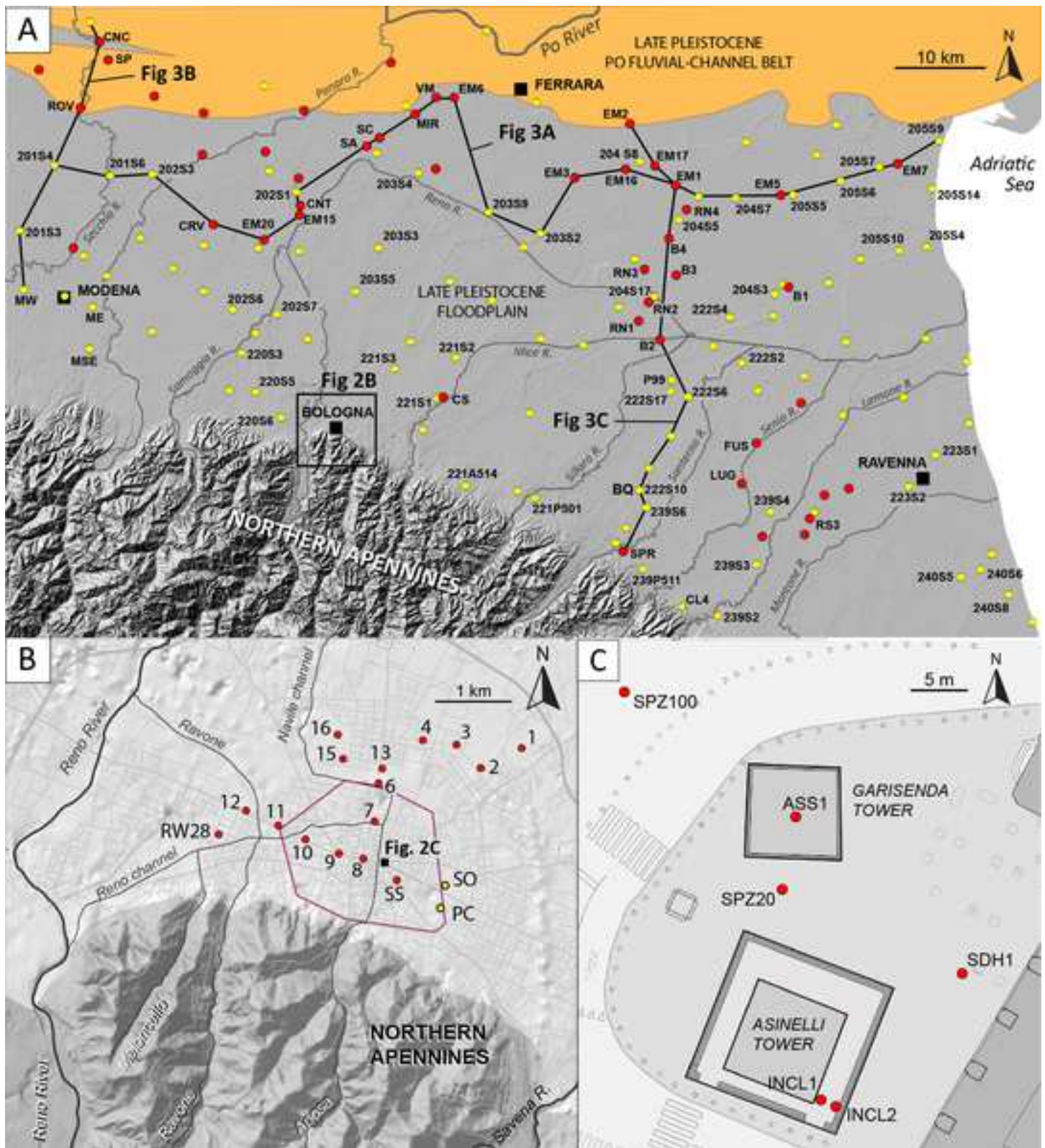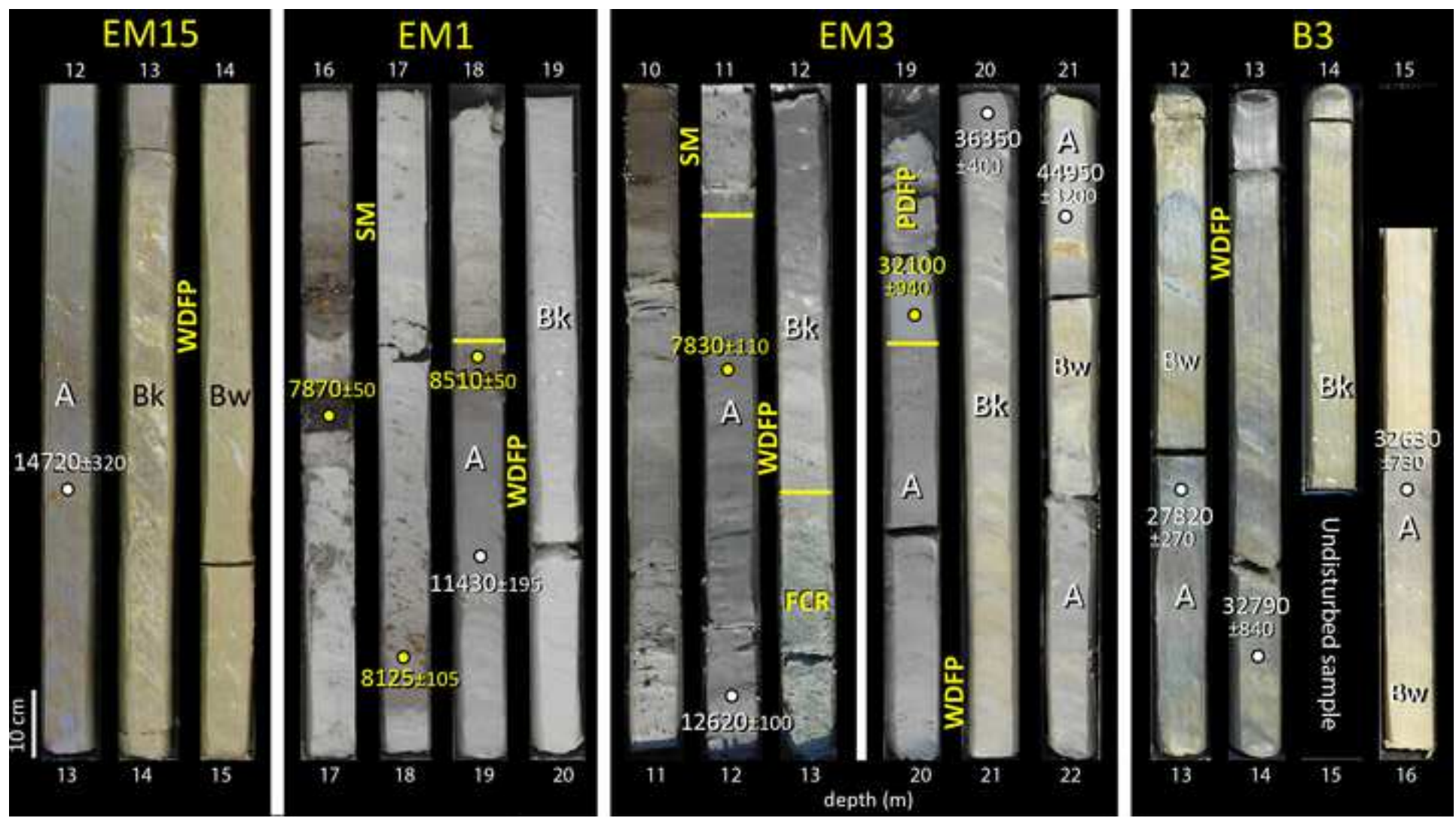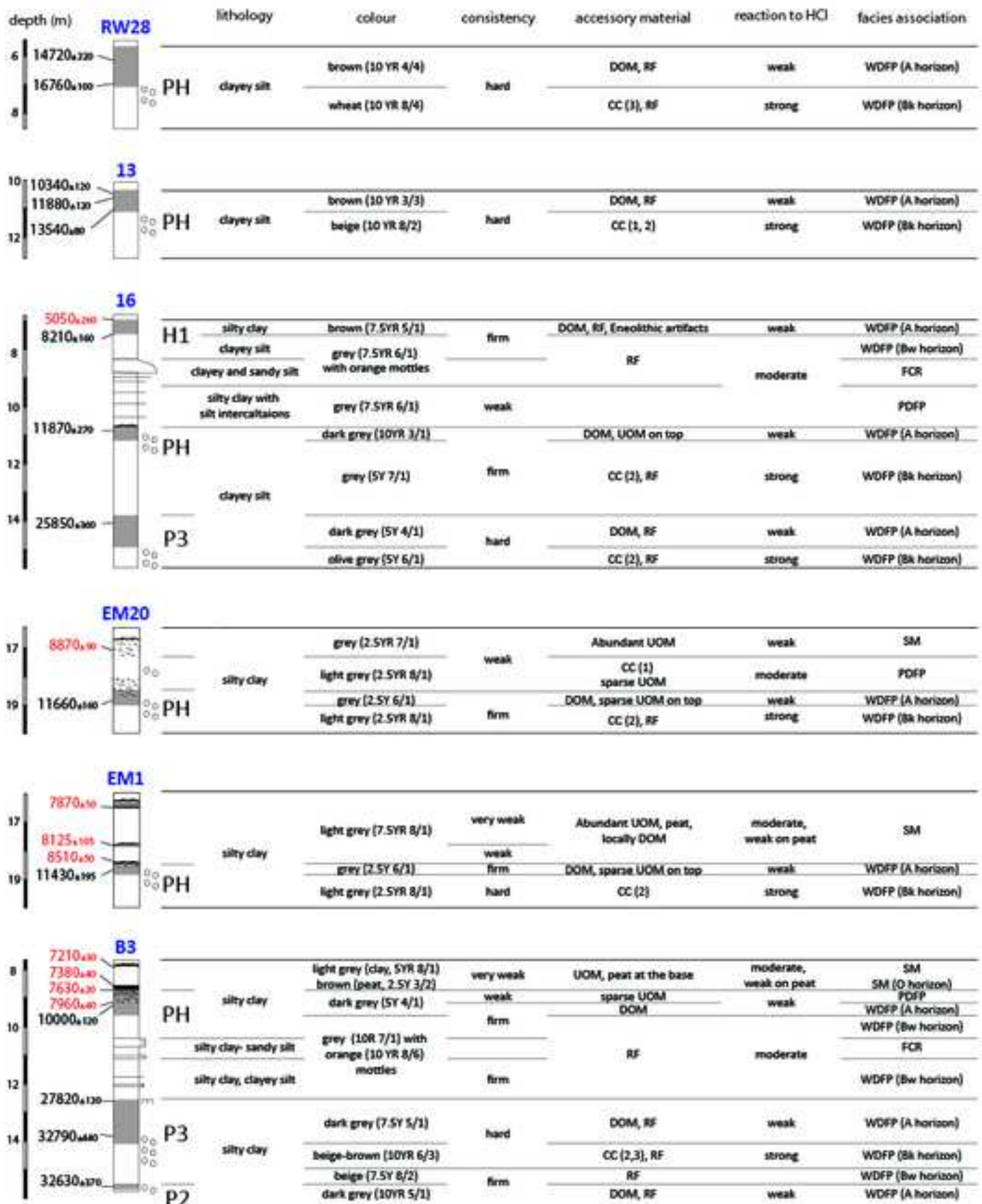| depth (m)		lithology	colour	consistency	accessory material	reaction to HCl	facies association
17 8870±90			grey (2.5YR 7/1)	weak	Abundant UOM	weak	SM
		silty clay	light grey (2.5YR 8/1)		CC (1) sparse UOM	moderate	PDFP
19 11660±660	PH		grey (2.5Y 6/1)		DOM, sparse UOM on top	weak	WDFP (A horizon)
			light grey (2.5YR 8/1)	firm	CC (2), RF	strong	WDFP (Bk horizon)

EM1

depth (m)		lithology	colour	consistency	accessory material	reaction to HCl	facies association
17 7870±50			light grey (7.5YR 8/1)	very weak	Abundant UOM, peat, locally DOM	moderate, weak on peat	SM
8125±105		silty clay		weak			
8510±50			grey (2.5Y 6/1)	firm	DOM, sparse UOM on top	weak	WDFP (A horizon)
19 11430±595	PH		light grey (2.5YR 8/1)	hard	CC (2)	strong	WDFP (Bk horizon)

B3

depth (m)		lithology	colour	consistency	accessory material	reaction to HCl	facies association
8 7210±60			light grey (clay, 5YR 8/1)	very weak	UOM, peat at the base	moderate, weak on peat	SM
7380±60			brown (peat, 2.5Y 3/2)				SM (O horizon)
7630±20		silty clay	dark grey (5Y 4/1)	weak	sparse UOM	weak	PDFP
7960±60	PH				DOM		WDFP (A horizon)
10000±120				firm			WDFP (Bw horizon)
10		silty clay- sandy silt	grey (10R 7/1) with orange (10 YR 8/6) mottles		RF	moderate	FCR
		silty clay, clayey silt		firm			WDFP (Bw horizon)
12 27820±130							
14 32790±440	P3		dark grey (7.5Y 5/1)	hard	DOM, RF	weak	WDFP (A horizon)
		silty clay	beige-brown (10YR 6/3)		CC (2,3), RF	strong	WDFP (Bk horizon)
32630±370			beige (7.5Y 8/2)	firm	RF		WDFP (Bw horizon)
	P2		dark grey (10YR 5/1)		DOM, RF	weak	WDFP (A horizon)

Figure 5

Click here to access/download;Figure;Fig. 5.jpg ±

Figure 6

Click here to access/download;Figure;Fig. 6.jpg

Figure 7

Figure 8   Click here to access/download;Figure;Fig. 8.jpg ⤓

13.4 radiocarbon date from the PH paleosol (cal kyr BP)   ○ core   ◇—◇ buried anticline
21.9 radiocarbon date below the PH paleosol (LGM SU)   ● core with radiocarbon dates

Figure 9

Figure 10

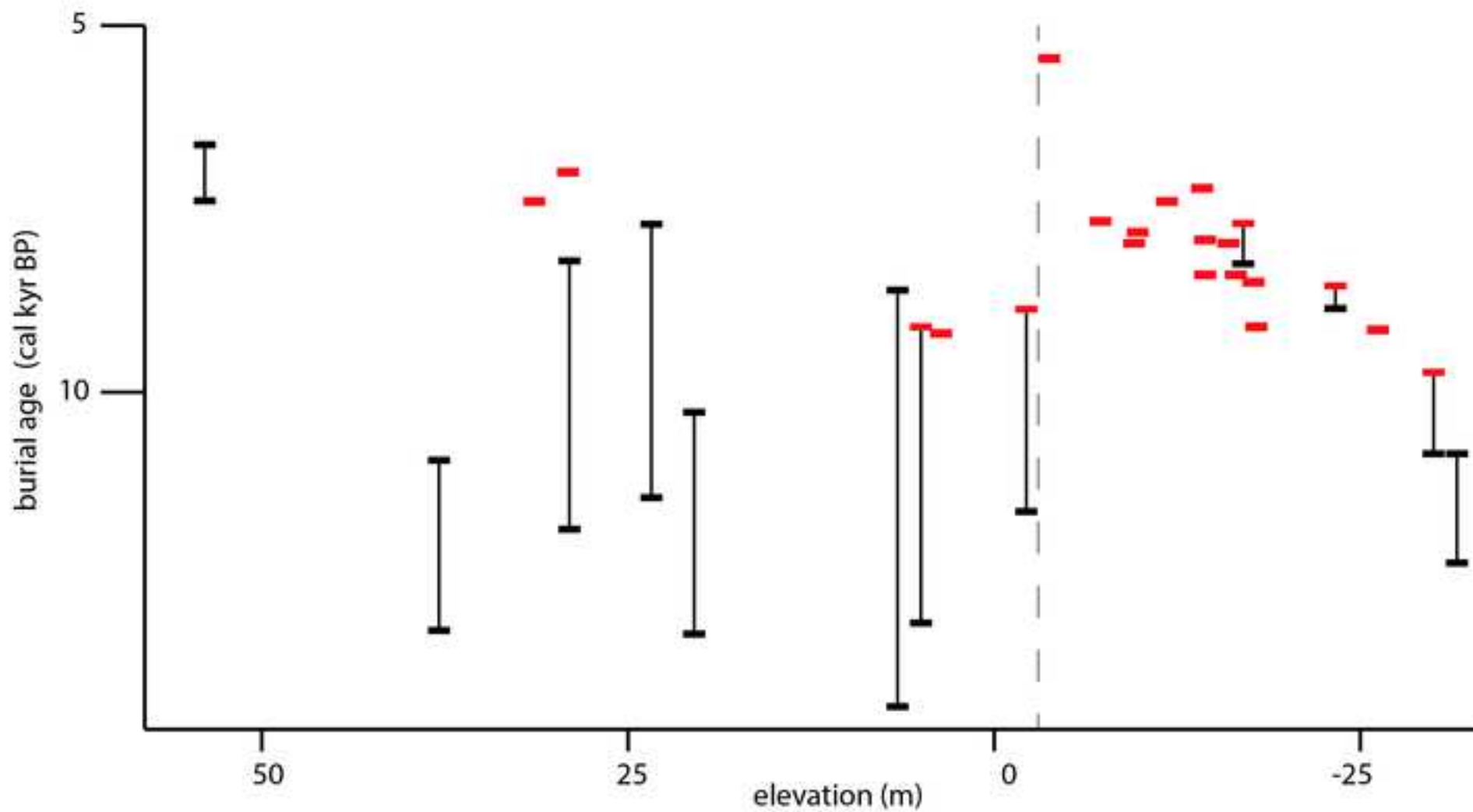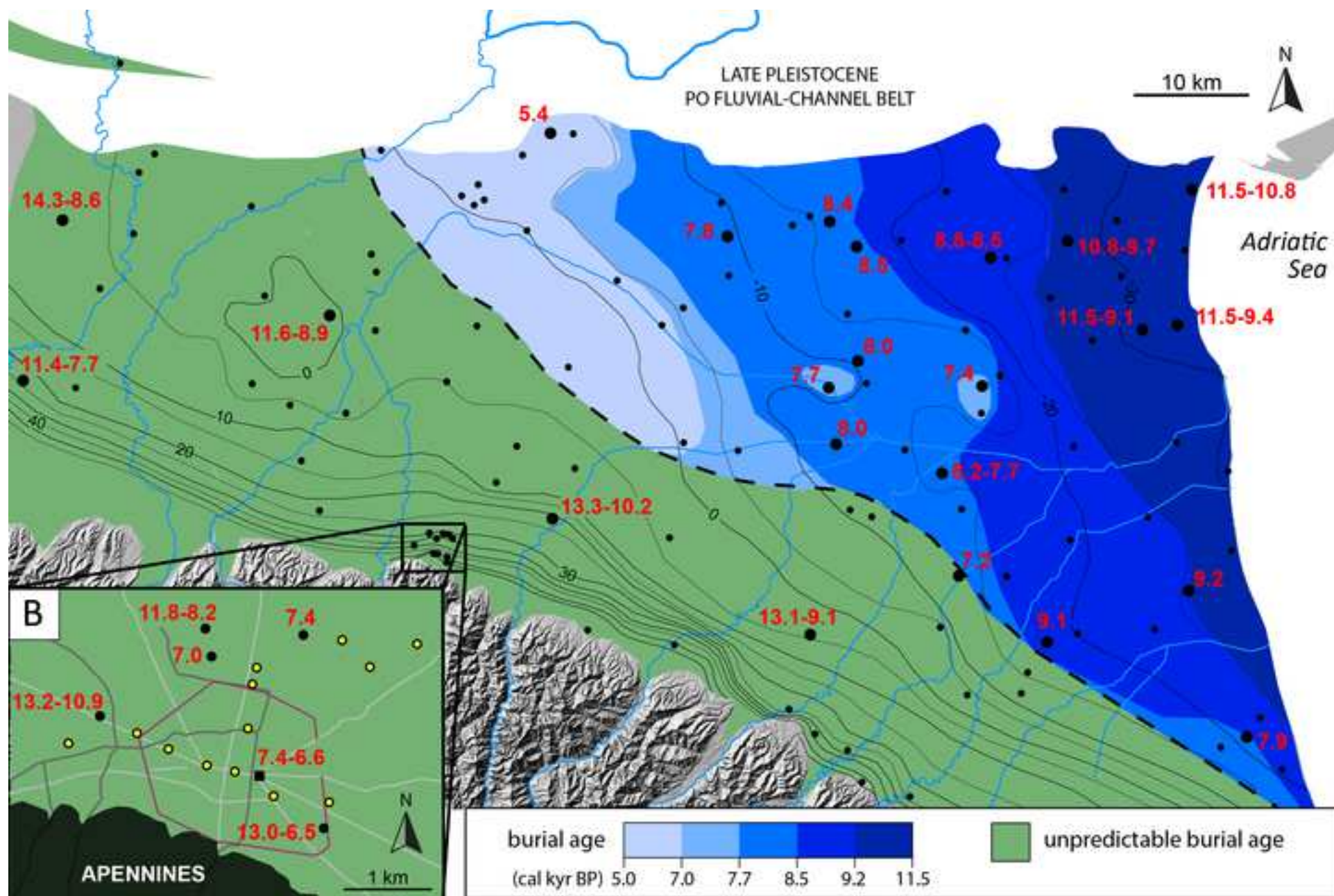Click here to access/download;Figure;Fig. 10.jpg

Figure 10

Declaration of interests

☒ The authors declare that they have no known competing financial interests or personal relationships that could have appeared to influence the work reported in this paper.

☐The authors declare the following financial interests/personal relationships which may be considered as potential competing interests: